Deep Sea Research Part I: Oceanographic Research Papers
February 2024, Volume 204, Pages 104230 (16p.)
https://doi.org/10.1016/j.dsr.2023.104230
https://archimer.ifremer.fr/doc/00870/98152/

Phytoplankton distribution under late summer conditions in the Algerian basin during SOMBA cruise (2014): Chemotaxonomy approach (CHEMTAX)

Aït-Kaci Malik [1,*], Louanchi Ferial [1], Keraghel Mehdia-Asma [1], Harid Romaissa [1], Zerrouki Mohamed [1], Mortier Laurent [2]

[1] ECOSYSMarL: Laboratoire des Écosystèmes Marins et Littoraux, ENSSMAL, Station de Recherche de Sidi Fredj, Algeria
[2] LOCEAN: Laboratoire D'Océanographie et Du Climat: Expérimentations et Approches Numériques, Unité Mixte de Recherche 7159 CNRS/IRD/Université Pierre et Marie Curie/MNHN, Institut Pierre Simon Laplace, Place Jussieu, 75252, Paris, France

* Corresponding author : Malik Aït-Kaci, email addresses : malik.ait-kaci@enssmal.edu.dz ; aitkaci.malix@gmail.com

f.louanchi@enssmal.dz ; asma.keraghel@enssmal.edu.dz ; r.harid@enssmal.dz ; m.zerrouki@enssmal.dz ; mortier@locean-ipsl.upmc.fr

Abstract :

Marine phytoplankton forms the basis of the marine food web. Its diversity (size and pigmentation) has a significant impact on biogeochemical processes such as photosynthetic efficiency, trophic interactions, and global carbon fluxes. To date, little is known about the Algerian Basin regarding phytoplankton quality and quantity. In this study, we analyzed the distribution of phytoplankton communities in the Algerian Basin based on HPLC/Chemotaxonomy analysis for the summer season of 2014. The chemical taxonomy software CHEMTAX v1.95 was used to estimate the contributions of various phytoplankton groups to total chlorophyll a (TChl a). The results showed that prymnesiophytes were the dominant group (16%) in the nanoplankton and occupied the entire water column, whereas cryptophytes were observed exclusively in the western region of the basin, and contributed about 6% to the TChl a. Diatoms had the highest contributions (18%) to the TChl a, and their emergence was linked to nutrient enrichment. Dinoflagellates had a contribution of about 12% with little variation throughout the basin. Prochlorococcus had a contributions of about 13% and prevailed in the deep layers (60–100 m) following the nitracline, while Synechococcus (11%) occupied the shallower layers (10–60 m) (beneath the MLD) following the nutrient depletion. Moreover, it is noteworthy that phytoplankton communities in the western part of the basin showed greater diversity and abundance, influenced by Atlantic waters and deep nutrient enrichment. In contrast, the eastern part of the basin displayed lower productivity, characterized by reduced diversity and the prevalence of nano- and picoplankton.

Highlights

► Phytoplankton communities in the Algerian basin are characterized by the CHEMTAX approach. ► Nano- and micro-phytoplankton prevail in the Algerian basin. ► Diatoms, prymnesiophytes, and *Prochlorococcus* are the major phytoplankton groups in the Algerian basin. ► Phytoplankton communities are more abundant and diverse in the western part of the Algerian basin compared to the eastern part. ► The composition of phytoplankton communities is linked to the physical-chemical dynamics of the Algerian basin.

Keywords : Phytoplankton, Phytoplankton pigments, Community composition, CHEMTAX, Algerian Basin, Western Mediterranean

1. Introduction

Marine phytoplankton provides the basis for the food web of sea species and contributes at least a quarter of the biomass of the world's vegetation. They play a major role in climatic processes by modulating the carbon cycle via the mechanisms of photosynthesis and respiration (Aiken et al., 1992). Photosynthetic activities bind atmospheric carbon dioxide (Chris and Feely, 2007) and phytoplankton sedimentation ensures fixed-carbon sequestration in the ocean's deep layers (Sabine et al., 2004).

The phytoplankton distribution in the ocean depends on their adaptation to several environmental key factors, including irradiance (Rodríguez et al., 2006; Schlüter et al., 2000), the spectral distribution of light (Wood, 1985), nutrient status (Hou et al., 2007; Kheireddine et al., 2017; Staehr et al., 2004), mixing regimes (Brunet et al., 2003; Thompson et al., 2007), temperature and salinity, which can vary horizontally and vertically. The vertical distribution of phytoplankton groups is determined by the vertical distribution of these physical-chemical factors. For example, phytoplankton growth may be nutrient-limited in the surface layers, while light may be the limiting factor in the deeper layers, resulting in a different taxonomic composition in the water column.

The role of the phytoplankton in marine ecosystems is affected by its taxonomic and size composition. The dominant cell size affects sinking and sequestration; large cells such as diatoms sink faster than smaller cells. This criterion is predominant in structuring pelagic ecosystems as it constitutes the base of the web food. The size of dominant phytoplankton affects the degree to which energy, carbon and nutrients are made available through phytoplankton production to higher trophic levels or export to deeper water or the sediment. Some prymnesiophytes can produce calcite, making them important contributors to the vertical flux of carbonate in the oceans (Broecker and Peng, 1982). The use of pigment data in the quantitative estimates of phytoplankton classes has become crucial as there is increasing evidence that each class exerts a unique role on the biogeochemical cycles in the ocean (Gibb et al., 2001).

The Mediterranean Sea (MS) is an oligotrophic region (Ignatiades, 2005; Krom et al., 1991; Thingstad et al., 2005). It is known as a Low-Nutrient-Low-Chlorophyll system and is characterized by a general west-to-east gradient increase of oligotrophy (Durrieu de Madron et al., 2011). In addition, the MS exhibits a rapid response to external conditions in comparison to the oceans (Crispi et al., 2001) because of its semi-enclosed nature, together with its smaller inertia due to the relatively short residence time of its water masses (Andrie and Merlivat, 1988; Bethoux, 1980; Durrieu de Madron et al., 2011). Local environmental

events such as wind mixing, hydrodynamic mesoscale processes, river inputs (Ludwig et al., 2010), and dry and wet atmospheric deposition play an important role in the local fertilization of the MS (Durrieu de Madron et al., 2011).

The Algerian Basin (AB) plays an important role in the western Mediterranean water circulation, biogeochemical cycles of nutrients, and the carbon system. In the western part, Atlantic waters enter Gibraltar and recirculate in meanders and eddies towards the Algerian coast around 0°E (Millot, 1987; Millot and Taupier-Letage, 2005; Puillat et al., 2002). To date, the effects of these complex features have been poorly studied in the AB (Moutin and Prieur, 2012). Much remains to be known concerning the interactions between the biogeochemistry of the AB and its circulation dynamics and ventilation (Tanhua et al., 2013), as well as its phytoplankton and trophic regimes.

Primary production in the AB may exhibit the following features: 1) two seasons of high and low biomass, separated by sharp transitions characterizing the offshore domain, 2) intense and distinct dynamics in the coastal area, representing 44% of the total phytoplankton biomass (Harid et al., 2022) that is characterized by a shorter and earlier production season in the eastern part of the basin compared to the western part (Benzouaï et al., 2020). The biological activity associated with chemical and physical carbon pumps resulted in anthropogenic carbon sequestration of about 0.44-0.53 PgC in 2014 (Keraghel et al., 2020). Several studies have addressed the horizontal partitioning of the Mediterranean (D'Ortenzio and Ribera d'Alcalà, 2009) in terms of phytoplankton community structure, but they have focused only on the very top layer and did not represent the AB, where high chlorophyll *a* (Chl *a*) values can be found at depth (Pujo-Pay et al., 2011; Raimbault et al., 1993).

This study is the first to be conducted in the AB, the southern part of the western Mediterranean. Unlike the Northwestern Mediterranean, little is known about phytoplankton quality and quantity in the AB. Apart from a few attempts to identify phytoplankton species along the Algerian coast (Illoul et al., 2008; Mustapha, 2021) and a few large-scale trials (Barlow et al., 1997; Garczarek et al., 2007; Moutin and Prieur, 2012), the AB remains the least studied area of the MS. In this work, we used pigments as chemotaxonomic markers for the first time in this region to calculate the contribution of individual phytoplankton groups to the total phytoplankton assemblage and to answer the following questions: Which phytoplankton groups are dominant in the AB during the summer? How are these groups distributed across the basin? How do the environmental parameters of the AB affect the phytoplankton distribution?

2. Materials and methods

2.1. Cruise strategy

Data were obtained during the SOMBA-GE cruise in the AB, conducted on the R/V Téthys II (CNRS-INSU) from August 14 to September 10, 2014. This cruise occurred in the framework of the MERMEX (Marine Ecosystems' Response in the Mediterranean Experiment Program) program, which aims to study the Mediterranean marine ecosystem and assess and predict its changes in the context of global warming and increasing anthropogenic pressure. The cruise covered the entire AB with 70 hydrological stations (Fig. 1).

2.2. Hydrography

Vertical profiles of temperature and salinity were measured at all the stations using a Sea-Bird SBE911 plus conductivity-temperature-Depth profiler (CTD) equipped with a Chlorophyll fluorescence sensor (Chelsea Acquatracka) and a dissolved oxygen sensor (SBE43). The accuracy for temperature and practical salinity measurements was ±0.002 °C and ±0.003, respectively. Discrete samples for biogeochemical parameters were collected using a carousel Niskin bottle system (11 bottles of 12 L). Daily discrete oxygen measurements by Winkler potentiometric method modified by Langdon (2010) served as calibration points. The precision of the measurements was about 1.6 µmol/kg.

Nutrient samples were collected in 15 ml acid-washed plastic vials at all hydrographical stations and poisoned immediately with mercuric chloride. The samples were analyzed by automatic colorimetric procedures using a Technicon AutoAnalyzer (Tréguer and Le Corre, 1975) in the MIO Laboratory (Mediterranean Institute of Oceanography-France). The precision (and detection limits) of the nitrite, nitrate, orthophosphate and silicic acid measurements were 2% (0.03 µM), 3-5% (0.05 µM), 3-5% (0.02 µM) and 5% (0.05 µM), respectively.

2.3. Pigments analysis

Pigment samples were collected on 44 stations, at a frequency of 6 samples per station: 5 levels in the first 100 m and one "dark" level. Surface sampling was tightened around the Deep Chlorophyll Maximum (DCM). Samples were filtered on 25 mm GF/F glass fiber, then frozen in liquid nitrogen (-80 °C) until analysis. Filters were placed in 3 ml of 100% methanol for two hours, disrupted by sonication twice, and clarified by filtration (GF/F Whatman).

Measurements were performed the same day by HPLC (HPLC 1200) at the Laboratoire d'Océanographie de Villefranche-France (LOV). The analytical procedure is described in Ras et al. (2008). The injection volume was reduced to 30 µL due to the high concentration of the extracts. Each extract was injected in triplicate. The detection of carotenoids and chlorophylls *c* and *b* was performed at 450 nm, chlorophyll *a* and derivatives at 676 nm, and bacteriochlorophyll *a* at 770 nm. The detection limit for 1 L filtered (in mg m^{-3}) was around 0.0001-0.0002 for all measured pigments. Calibration precision and accuracy were about 0.4% and 0.3%, respectively.

Quality control was applied to pigment data following the procedure described by Aiken et al. (2009). Relationships between total chlorophyll *a* (TChl *a*) and accessory pigments (AP) were examined. The statistical criteria for the quality assurance for the pigment data were:

(1) The difference between TChl *a* and AP should be less than 30% of the total pigment concentration.

(2) The regression between TChl *a* and AP should have a slope within the range of 0.7–1.4 and must explain more than 90% of the total variance ($r^2 > 0.9$).

Our data showed that the difference between TChl *a* and AP was always less than 30% of the total pigments (TP) concentration, and there was a regression between TChl *a* and AP with r^2 value of 0.95 and a slope of 1.03.

2.4. CHEMTAX analysis

In this study, CHEMTAX v1.95 chemical taxonomy software (Mackey et al., 1996) was used to estimate the contributions of various phytoplankton classes to the TChl *a* in the AB. CHEMTAX uses factor analysis and a steepest descent algorithm to find the best fit to the data based on an initial guess of the pigment ratios for the classes to be defined (Mackey et al., 1996; Wright et al., 1996). The data matrix (S) of pigment concentrations must be factorized into two matrices, (F) giving the ratios of different pigments for each phytoplankton class, and (C) giving the abundances of each phytoplankton class in each sample (Mackey et al., 1996).

2.4.1. Cluster analysis

In the CHEMTAX procedure, cluster analysis can be used to subdivide pigment data into clusters representing ecological or geographic provinces by water mass properties. Indeed, the AB is characterized by the presence of two surface water masses, the Atlantic waters (AW) penetrating from the Alboran Sea, less salty and colder than the resident modified Atlantic waters (MAW) that are saltier and warmer (Millot, 1999) (for more details, see

194 section 4.1). In addition to the salinity and temperature differences, the nutrient budget
195 decreases eastward, corresponding to the oligotrophy gradient described by many authors
196 in the MS (e.g. Pujo-Pay et al., 2011). As a result, it was determined that coherent sub-sets
197 of samples with similar array of environmental conditions were required to provide
198 consistency of pigment ratios across all samples in a data group.
199 Two clusters were defined based on a principal components analysis (PCA) that combined
200 temperature, salinity, and nutrients data of all stations: Cluster 1, comprising 28 stations
201 representing the MAW water mass, and Cluster 2, with 16 stations representing the AW
202 water mass (Fig. 2). Following the recommendation of Mackey et al. (1996), the chosen
203 number of stations per sub-group was suitable for running CHEMTAX analysis.
204 Subsequently, we examined the pigment and taxonomic composition of these water masses.

205 ### 2.4.2. CHEMTAX parametrisation

206 Based on the pigments detected during the cruise and previous studies in the western
207 Mediterranean, we considered 10 phytoplankton groups and 14 pigments to avoid the
208 linearity of the initial pigment ratio matrix F_0, as recommended by Mackey et al. (1996). The
209 F_0 matrix (Table 1a) was constructed using literature values from Mackey et al. (1996) and
210 Higgins et al. (2011). We set the ratio limit matrix to the default value (500%), allowing the
211 initial pigment ratio, r, to vary from r/6 to 6r.
212 Two types of data matrices (S) were used: integrated concentrations and concentrations
213 with depth. First, we applied CHEMTAX on the integrated concentrations, and following
214 Latasa (2007), successive runs using the output from each run as the input for the next one
215 were performed. In a second phase, CHEMTAX was applied on concentrations with depth
216 for the entire data set. The initial ratio matrix (F_0) for this phase was derived from the final
217 ratio matrices obtained for clusters 1 and 2 after analysis (optimized ratios) (refer to Table
218 1b, c). The data set was divided into depth strata (0-20 m, 20-40 m, 40-60 m, 60-80 m, 80-
219 120 m) due to the strong stratification of the water column during the cruise period and the
220 large number of samples. Whether for integrated concentrations or concentrations with
221 depth, data from each cluster were run separately to minimize potential variations in the
222 CHEMTAX optimization procedures.
223 For all CHEMTAX runs, a series of 60 pigment ratio matrices were generated by multiplying
224 each ratio from the initial matrix by a random function to optimize the matrix, and 10% (n=6)
225 of the generated ratios with the lowest root-mean-square residual were averaged. For more
226 procedure details, see Wright et al. (2009). The solution with the smallest residual was used
227 for the estimated taxonomic abundance. Chl *a* was used for calculating the biomass of all

groups, except *Prochlorococcus*, for which divinyll chlorophyll *a* (DVChl *a*) was used. The optimized ratios were not altered considerably from starting ratios and compared well with the range values that Higgins et al. (2011) described.

Table 1: Ratio matrices used in CHEMTAX analysis: a) initial ratios before analysis, b) optimized ratios after analysis (Cluster 1), c) optimized ratios after analysis (Cluster 2).

Marker pigments	PERI	BUT	FUCO	HEX	NEOX	PRAS	VIOL	DDX	ALLO	ZEA	DVChl*b*	Chl*b*	DVChl*a*	Chl*a*
Class														
(a) Initial Ratio matrix														
Synechococcus	0	0	0	0	0	0	0	0	0	0.636	0	0	0	1
Prochlorococcus	0	0	0	0	0	0	0	0	0	0.321	1.074	0	1	0
Diatoms	0	0	0.623	0	0	0	0	0.163	0	0	0	0	0	1
Pelagophytes	0	0.658	0.779	0	0	0	0	0.191	0	0	0	0	0	1
Prymnesiophytes	0	0	0	1.708	0	0	0	0.101	0	0	0	0	0	1
Cryptophytes	0	0	0	0	0	0	0	0	0.379	0	0	0	0	1
Dinoflagellates	0.558	0	0	0	0	0	0	0.253	0	0	0	0	0	1
Euglenophytes	0	0	0	0	0.068	0	0	0.251	0	0	0	0.377	0	1
Clorophytes	0	0	0	0	0.066	0	0.049	0	0	0.032	0	0.315	0	1
Prasinophytes	0	0	0	0	0.063	0.245	0.054	0	0	0	0	0.704	0	1
(b) Final Ratio matrix (Cluster 1)														
Synechococcus	0	0	0	0	0	0	0	0	0	0.594	0	0	0	1
Prochlorococcus	0	0	0	0	0	0	0	0	0	0.252	0.959	1	1	0
Diatoms	0	0	0.634	0	0	0	0	0.021	0	0	0	0	0	1
Pelagophytes	0	1.158	0.509	0	0	0	0	0.039	0	0	0	0	0	1
Prymnesiophytes	0	0	0	1.155	0	0	0	0.069	0	0	0	0	0	1
Cryptophytes	0	0	0	0	0	0	0	0	0.278	0	0	0	0	1
Dinoflagellates	0.677	0	0	0	0	0	0	0.119	0	0	0	0	0	1
Euglenophytes	0	0	0	0	0.028	0	0	0.436	0	0	0	0.39	0	1
Clorophytes	0	0	0	0	0.056	0	0.019	0	0	0.049	0	0.502	0	1
Prasinophytes	0	0	0	0	0.099	0.257	0.074	0	0	0	0	0.575	0	1
(c) Final Ratio matrix (Cluster 2)														
Synechococcus	0	0	0	0	0	0	0	0	0	0.526	0	0	0	1
Prochlorococcus	0	0	0	0	0	0	0	0	0	0.439	0.121	0	1	0
Diatoms	0	0	0.605	0	0	0	0	0.035	0	0	0	0	0	1
Pelagophytes	0	1.833	0.473	0	0	0	0	0.043	0	0	0	0	0	1

Prymnesiophytes	0	0	0	1.424	0	0	0	0.062	0	0	0	0	0	1
Cryptophytes	0	0	0	0	0	0	0	0	0.278	0	0	0	0	1
Dinoflagellates	0.603	0	0	0	0	0	0	0.102	0	0	0	0	0	1
Euglenophytes	0	0	0	0	0.024	0	0	0.462	0	0	0	0.334	0	1
Clorophytes	0	0	0	0	0.063	0	0.023	0	0	0.023	0	0.583	0	1
Prasinophytes	0	0	0	0	0.11	0.285	0.08	0	0	0	0	0.624	0	1

Pigment abbreviations: PERI: Peridinin, BUT: 19'-Butanoyloxyfucoxanthin, FUCO: Fucoxanthin, HEX: 19'-Hexanoyloxyfucoxanthin, NEOX: Neoxanthin, PRAS: Prasinoxanthin, VIOL: Violaxanthin, DDX: Diadinoxanthin, ALLO: Alloxanthin, ZEA: Zeaxanthin, DVChlb: Divinyl Chlorophyll b, Chlb: Chlorophyll b, DVChla: Divinyl Chlorophyll a, Chla: Chlorophyll a.

2.5. Photo-pigment indices

The main role of the pigment Chl *a* is to absorb light for photosynthesis. Additional accessory pigments (Chls *b* & *c*) and various carotenoids can extend the phytoplankton's light-harvesting spectrum, ensuring optimal absorption efficiencies (Kirk, 1994). However, other carotenoids protect the photosynthetic apparatus against high irradiance (Kirk, 1994). The phytoplankton can change the structure of the community, and hence pigment ratios, as adaptive strategies to survive in the environment. Accordingly, phytoplankton pigments and ratios can be used to assess changes in phytoplankton community structure and/or physiological responses to environmental conditions.

As pigment concentrations and composition of phytoplankton may be altered in response to environmental conditions (nutrient availability and irradiance intensity) (Higgins et al., 2011), photo-pigment indices were calculated according to Barlow et al. (2007) and used to assess the changing contribution of chlorophylls and carotenoids to the total pigment pool. Carotenoids were separated as photosynthetic (PSC) including PERI, FUCO, HEX, BUT, and photoprotective (PPC) including ALLO, DDX, Diatoxanthin, VIOL, ZEA, Lut, the sum of carotenes (β, β & β,ε). Chlorophylls were separated as follows: TChl*a* (Chl *a* + DVChl *a*), TChl*b* (Chl *b* + DVChl *b*), and TChl*c* (Chl c_1c_2 + Chl c_3). Accordingly, five photo-pigment indices were defined and symbolized as (PSC/Tpig), (PPC/Tpig), (TChla/Tpig), (TChlb/Tpig), and (TChlc/Tpig).

3. Results

Hydrology and biogeochemical parameters, along with pigment distribution, are shown on two transects: the west-east (WE transect), and the east-northeast (ENE transect). These transects cover the AB with 29 stations and represent the major physical structures observed during the cruise.

3.1. Environmental conditions

The SOMBA cruise was conducted in late summer. This period of the year is usually characterized by strong stratification induced by high temperatures in the AB. Here we describe the physical and chemical conditions of the basin during the cruise.

3.1.1. Sea Surface Salinity

Fig. 2 shows the surface salinity for the cruise period. The AW enters the Algerian Basin from the Alboran Sea with salinities of about 36.8 (and temperatures of 18.5° C). This water mass first mixes with water of higher salinity and temperature (about 37.37 and 25° C, respectively) toward 2° E longitude. Then two filaments break off, one heading northwest and the other northeast (reaching stations located at 37.8° N and 38.9° N in the basin's eastern and western parts), and mix with resident Mediterranean water. The maximum salinity found was 38.5 at the easternmost point of the basin.

3.1.2. Temperature

The temperature distribution over the two transects is shown in Fig. 3A. The mean surface temperature recorded during the SOMBA cruise was about 24.8 °C. In the west, this warm layer was restricted to the first 20 m, apparently due to the significant upwelling of cold water (<15 °C) reaching a depth of 50 m. In contrast, the thickness of the warm surface layer (20-22.5 °C) reached depths of 40 m to the east. At stations 2-3, 2-2, and 2-1, we observed the downwelling of surface water with temperatures higher than 15 °C to depths below 100 m. On the ENE transect, the surface layer (0-50 m) was characterized by high temperatures (20-25 °C). Another upwelling event of cold deep water (15 °C) was observed at stations 4-7, 4-6, 4-5, and from station 4-11 to the northeast, rising to depths of 80 m.

3.1.3. Column stability and mixed layer depth

Below 40 m depth, the water column was characterized by stratification that reflected the presence of the eddies mentioned above. In the western part, shoaling isopycnals reaching 40 m depth were observed at stations 3-8, 3-10, and affected the adjacent stations 3-3, 3-7 (Fig. 3B). This upwelling could be linked to the presence of a cyclonic eddy in this area (Fig. 1). In the eastern part, an anticyclonic eddy was identified by the deepening of the density anomaly and isotherms between 5 and 6.75° E (2-4, 2-3, 2-2, and 2-1) (Fig. 3A, B). The eddy's footprint was still visible down to 120 m. Shoaling isopycnals were also observed further east (from station 1-13), approaching the Sardinian coast and reaching a depth of 50 m, seemingly in relation to the Sardinian Eddies. Density and temperature isolines rose at

stations 4-7, 4-6, 4-5 (east) and from station 4-11 (northeast), demonstrating the instability that prevailed in this part of the basin.

Relative stratification was observed in the basin's central part, which discontinued in the ENE transect. Indeed, the transect went through instabilities visible on the SLA map (Fig. 1) where cyclonic eddies induced shallower density isolines (stations 4-7, 4-12, Fig. 3B).

In the western part of the basin, the MLD was located around 12 m. The thickness of the mixed layer increased to 20 m in the central part (stations 3-10, 2-15 and 4-3, 4-4, 2-4) and to 30-40 m in the eastern part, at stations 2-3, 2-2, 2-1 and 4-5 slightly enhanced by the persistent anticyclonic eddy (at 6° E) (Fig. 3B). Along the ENE transect, the MLD deepened from 12 m (station 1-16) to 25 m (stations 4-8, 4-7), slightly shallowing northward to around 15 m depth.

3.1.4. Nutrients

The distribution of nitrate NO_3^-, phosphate PO_4^{3-}, and silicate $Si(OH)_4$ is shown in Fig. 3C, D, and E. In the western part of the basin, the upward movement of deep water combined with the penetration of the AW from the Alboran Sea lead to the enrichment of the surface waters (20 m-60 m, stations 3-3, 3-7, 3-8) with maximal values of about 1 µmol/l, 0.1 µmol/l, and 3 µmol/l for NO_3^-, PO_4^3, and $Si(OH)_4$, respectively. Thereby, shallow nutriclines were detected in this area. Eastward, the upper layer (0-70 m) was nutrient depleted with NO_3^- and PO_4^{3-} concentrations close to the detection limit. The top of nutriclines deepened eastward from 40 m to 75 m and from 20 m to 100 m for NO_3^- and PO_4^{3-}, respectively (Fig. 3C, D), corresponding to the eastward Mediterranean oligotrophy gradient. Whereas, an abundance of silicate was observed east of the basin with values of about 1 µmol/l in the upper layer. The nutrient concentrations increased below 80 m depth to 6 µmol/l, 0.2 µmol/l, and 3.5 µmol/l for NO_3^-, PO_4^{3-}, and $Si(OH)_4$, respectively. A less significant nutrient enrichment from deep waters was observed in the east (S1-11) around stations with shallow isopycnals (Fig. 3B), where the nutrient concentrations increased to around 0.4 µmol/l, 0.05 µmol/l and 1.5 µmol/l for NO_3^-, PO_4^{3-}, and $Si(OH)_4$, respectively, resulting in the nutricline to reach depths of 50 m (Fig. 3C, D, E).

The nutrient depletion was more pronounced along the ENE transect (down to 85 m depth), with nutricline deepening northward. The phosphacline (40-130 m) was located below the nitracline (40-100 m). The abundance of silicate persisted with maxima located deeper (below 80 m depth) than in the WE transect. Below this depleted nutrient layer, nutrient concentrations rose to values of about 4 µmol/l, 0.1 µmol/l, and 2 µmol/l for NO_3^-, PO_4^{3-}, and $Si(OH)_4$, respectively.

A particular observation was noted at the end of the ENE transect where a rise of nutrient concentrations occurred in shallow depths (stations 4-12, 4-13, and 4-14), seemingly related to the proximity of the island of Menorca.

3.1.4.1. N:P ratios

The molar nitrogen to phosphorous (N:P) ratio was calculated using the slope of N vs. P for the surface waters following the methodology outlined by Kress and Herut. (2001). In the upper water layer of the AB (down to 120 m depth), the N:P ratio ranged between 0 and 93. Fig. 4 shows the vertical distribution of the N:P ratio within the first 120 m, revealing three distinct layers: the nutrient-depleted layer (0-55 m) with the lowest N:P ratios (< 21), the layer between 60-75 m where N:P values reached a maximal value of 35, and the layer between 80-120 m where the variability in the N:P ratios was the highest (4-93). This distribution is typical for the MS, where a high variability of the N:P ratio is observed in the surface layer, as mentioned by several authors (Marty et al., 2008; Pasqueron de Fommervault et al., 2015; Schroeder et al., 2010).

Table 2: N:P ratios calculated for the west, east, and entire basin.

	West	East	Entire basin
Slope	19.9	24.6	22.6
Intercept	0.12	0.05	0.1

The observed N:P ratios showed a difference between the western and eastern parts of the AB, with values of 19.9 and 24.6, respectively (Table 2). The intercepts indicate a concentration of 0.12 µM and 0.05 µM when phosphate was exhausted in the western and eastern parts of the basin, respectively. The ratio observed in the eastern part is close to that reported by Pujo-Pay et al. (2011) for the euphotic zone in the western Mediterranean.

3.2. Pigments and phytoplankton distribution

3.2.1. Phytoplankton pigments

A total of 22 phytoplankton pigments were identified in this study. The dynamic of the major pigments was examined based on their vertical distribution through the WE transect and ENE transect (Fig. 5).

The TChl *a* concentration deepened eastward following the nutricline and light attenuation as implied by Mignot et al., (2014). In the western part, the TChl *a* maximum was located at about 20-35 m depth (stations 3-3, 3-7) (called hereafter western deep maximum, WDM) and, to a lesser extent, around 100 m depth (station 3-7). In the central part, the maximum

was found at 35-50 m (station 2-19) (first central deep maximum, CDM1) and 60 m (stations 4-3, 4-4) (second central deep maximum, CDM2). The TChl *a* maximum reached the depth of 75 m in the eastern part at station 1-11 (eastern deep maximum, EDM).

In the ENE transect, the maximal concentrations were located at 60 m depth (1-15, 4-11) and deepened northward to reach 70 m depth (4-14).

The distribution of HEX followed that of TChl *a*, except for its absence in the WDM at 100 m depth. The HEX maximum was linked to CDM2 (station 4-4) and a lesser extent, the northern maximum at station 4-11. The BUT pigment levels were also significant but generally lower than HEX. The findings showed that the pigment BUT persisted at depth after HEX's disappearance, in parallel to a nitrate peak, increasing the BUT/HEX ratio with depth and indicating the importance of pelagophytes at depth. FUCO presented a specific distribution and followed the TChl *a* west-east deepening trend. The maximal concentrations were observed in the nutrient-enriched waters of the basin and followed that of TChl *a*, especially in the east (EDM).

PERI presented the same evolution as TChl *a* except for its absence in the WDM (100 m). Maximal concentrations corresponded to WDM, CDM1, CDM2, and the northern TChl *a* maxima (stations 4-1, 4-14).

The ZEA distribution differed from that of TChl *a.* Indeed, the ZEA pigment was found in the surface layers of the basin, above the nutricline. The maximal concentrations deepened from 10 m in the west (stations 3-3 and 3-7) to reach 40-50 m depth east of the basin. DVChl *a* followed a specific distribution; the maximal concentrations were located at the 50-80 m depth layer for the WE transect in the central and eastern parts (stations 4-4, 2-1) and deepened northward from 50 to 95 m at stations 1-15 and 4-13, respectively. DVChl *b* stood out for its deep presence (70-100 m) markedly in the western and northern-east parts of the basin. DVChl *a* and *b* were found in the zone of nitrate accumulation where N:P ratios reached values of 40.

Chl *b* followed the TChl *a* distribution in the basin. We note the presence of small amounts of lutein, violaxanthin, neoxanthin, and prasinoxanthin, which had the same distribution as Chl *b*, indicating the presence of chlorophytes, prasinophytes, and euglenophytes (Jeffrey and Vesk, 1997). Regarding the rest of the pigments (BUT, DDX, Chlorophyll c_1c_2, Chlorophyll c_3, ALLO), they followed the same evolution as the TChl *a* with maximal concentration generally corresponding to that of TChl *a* except for ALLO which appeared exclusively in the western part of the basin (stations 3-3 and 3-7).

3.2.2. Photo-pigment indices

The AB was divided into four key regions (West, Central, East, and Northeast), and data within each region were averaged to facilitate straightforward comparisons. The western and central sectors included stations from Cluster 1 (MAW) and Cluster 2 (AW), while the eastern and northeastern sectors included only stations from Cluster 1 (MAW). Fig. 6 shows the distribution of photopigment indices with depth in these four regions representative of the AB.

The TChla/Tpig ratio showed a consistent stability with depth throughout the basin, with average values around 0.47. The most significant variation occurred in the surface layer of the western region, ranging from 0.48 to 0.57 (Fig. 6A, B).

Throughout the basin, there was a consistent decrease in the PPC/Tpig ratio with increasing depth. Notable variations were particularly evident in the 0-20 m layer of the western and central regions, where maximum values of 0.3 and 0.35 were observed (Fig. 6A, B). Beyond 50 m, the values remained relatively stable, fluctuating between 0.03 and 0.15. ALLO and ZEA were the most abundant pigments in the western surface layer of the basin and contributed with high proportions to the PPCs (32% and 34%, respectively), reflecting a high contribution of cryptophytes and *Synechococcus* and/or prasinophytes to the phytoplankton biomass.

Unlike the PPC/Tpig ratio, the PSC/Tpig ratio increased consistently with depth throughout the basin. Lower values were found in the surface layers of the western and central regions, ranging from 0.12 to 0.18. Meanwhile, values in the eastern and northeastern areas were approximately 0.22 to 0.25 and remained relatively constant with depth (Fig. 6C, D). Notable variations occurred in the western and central sectors of the basin below 20 meters, where ratios reached approximately 0.28. At a depth of 100 meters, maximum values (about 0.30) were reached for all four regions of the basin. The highest contributions to the PSCs were made by the pigment HEX (41% vs. 17% for BUT) in the western and central parts of the basin, while in the eastern and northeastern parts, HEX (17%) and FUCO (15%) were the major contributors to the PSCs compared to BUT (9%).

Throughout the basin, the 0-60 m layer showed consistently low values for both TChl*b* and TChl*c* (<0.1) with minimal variation and a slight increase in value with depth. Significant changes were observed only below 60 m depth, especially at the DCM. Marked changes were observed in TChl*b*, particularly in the eastern and northeastern regions of the basin, with maximum values of 0.18 and 0.26, respectively (Fig. 6C, D).

3.2.3. Vertical distribution of phytoplankton groups

Fig. 7 shows the vertical distribution of phytoplankton groups (as TChl a concentration derived from CHEMTAX) in the four representative AB regions. In the western part of the basin and for Cluster 1 (MAW) (Fig. 7A), the surface layer (0-20 m) was predominantly occupied by *Synechococcus* and prymnesiophytes. As the depth increased (30-40 m), *Prochlorococcus* became the dominant picoplankton group, while prymnesiophytes and dinoflagellates continued to be significant components of the community. In the DCM layer (50-70 m), diatoms emerged as the prevailing group, exhibiting higher abundance compared to other phytoplankton groups, such as *Prochlorococcus*, clorophytes, and pelagophytes. Below 70 m depth, the phytoplankton biomass decreased. However, diatoms and *Prochlorococcus* remained prominent components. Cluster 2 (AW) showed a significant prevalence of cryptophytes in the upper 30 m water column, exceeding the abundance of diatoms, dinoflagellates, and prasinophytes. Below this layer, the composition of the phytoplankton community shifted, and the dominant groups were prymnesiophytes, chlorophytes, and diatoms.

In the central part of the basin and for Cluster 1 (Fig. 7C), the upper layer (0-30 m) was dominated by *Synechococcus* and prymnesiophytes. At depths between 40-50 m, *Prochlorococcus*, prymnesiophytes, and dinoflagellates were the predominant groups, while diatoms, prasinophytes, and clorophytes exhibited lower abundance. At depths beyond 60 m, diatoms became the predominant group, alongside *Prochlorococcus* and prymnesiophytes, while pelagophytes and clorophytes persisted. In Cluster 2 (Fig. 7D), the layer between 10-20 m was dominated by *Synechococcus*, while cryptophytes, dinoflagellates, and pelagophytes prevailed at a depth of 30 m. At the DCM, the phytoplankton community consisted mainly of prymnesiophytes, diatoms, and dinoflagellates, with a lower abundance of *Prochlorococcus*, pelagophytes, and prasinophytes. The same groups were present below the DCM, with the appearance of clorophytes.

The surface layer (10-40 m) of the eastern part of the basin was primarily dominated by prymnesiophytes and *Synechococcus*, with *Prochlorococcus*, dinoflagellates, and euglenophytes being present to a lesser extent (Fig. 7E). At a depth of 50-60 m, clorophytes appeared along with *Synechococcus*, *Prochlorococcus*, prymnesiophytes, and dinoflagellates. At 70-80 m, a similar assemblage was observed, with diatoms becoming the major group, and pelagophytes/clorophytes exhibiting a higher abundance. Diatoms persisted deeper down and were the primary occupants of the deep layer.

Distinct variations in the phytoplankton community with depth were observed in the north-eastern region (Fig. 7F). In the 10-40 m layer, the phytoplankton community consisted mainly of prymnesiophytes, while in the 50-60 m layer, it was composed of prymnesiophytes, clorophytes, dinoflagellates, *Synechococcus*, and *Prochlorococcus*. At a depth of 70 m, *Prochlorococcus* was more abundant than *Synechococcus.* The community mainly consisted of clorophytes, diatoms, pelagophytes, and prymnesiophytes. *Prochlorococcus* became the dominant group in the community at deeper depths.

4. Discussion

4.1. Oceanographic conditions

The surface layer (0-150 m) of the AB is characterized by the AW which penetrates from the Almeria-Oran front, with a salinity of about 36.7. The AW flows eastward along the Algerian coast and forms the Algerian Current (AC), as described by Millot. (1985). Passing 0° longitude, the AW undergoes the mesoscale instabilities that characterize the AB, and filaments extend northward into the basin, seemingly in relation to the cyclonic and anticyclonic eddies shown in Fig. 1, as described by Morán et al. (2001).

Active mesoscale activity was observed in the basin during the SOMBA cruise, as shown in Fig. 1. This activity is marked to the east, off the Algerian slope, by events that could be more similar to open sea eddies with a hydrographical structure indicative of an anticyclonic motion, as mentioned by Millot. (1999) (large elevations of the sea surface, 10-20 cm, Fig. 1). Puillat et al. (2002) have also evidenced the cyclonic circuit of the AEs in the east of the AB. Testor and Gascard. (2005) have observed the formation of Sardinian Eddies (SEs) with a westward, cross-shelf, eddy-driven transport of LIW from the South Sardinia vein towards the interior of the AB following the periphery of the Algerian Gyres (Mallil et al., 2022). Therefore, the eastern part of the AB is one of the most energetic (at mesoscale) areas in the whole MS (Millot, 1999).

The AC instability highlighted in this work is consistent with other data analyzed by several authors (Font et al., 2004; Fuda et al., 2000; Millot, 1999; Olita et al., 2010). The Algerian eddies (AEs) can have a strong influence on the circulation of the entire AB, with marked signals on the distribution of water masses and biochemical parameters, and hence on ecosystems (Cotroneo et al., 2016), and can modulate biological activity (Olita et al., 2010; Taupier-Letage et al., 2003).

4.2. Phytoplankton contribution to TChl *a*

The relative contribution of phytoplankton to TChl *a* allowed us to investigate the distribution of the phytoplankton community in the AB during the summer of 2014. Clusters 1 and 2 (representative of the MAW and AW water masses, respectively) showed several differences and similarities. Within the nanoplankton, prymnesiophytes were the most abundant group in the basin (16% for both clusters) (Fig. 8 and Table 3). The latter results are similar to other studies in the MS (Barlow et al., 1997; Bustillos-Guzman et al., 1995; Claustre et al., 1994; Marty et al., 2008; Vidussi et al., 2001). Our results confirm the ubiquity of this algal class as in many other areas: the Atlantic Ocean (Barlow et al., 1993; Claustre and Marty, 1995; Gibb et al., 2001), the Pacific Ocean (Everitt et al., 1990; Miranda-Alvarez et al., 2020; Ondrusek et al., 1991), and the North Sea (Gieskes and Kraay, 1986).

Clorophytes and pelagophytes contributed more to TChl *a* in Cluster 1 than in Cluster 2 (12% - 8% and 9% - 6%, respectively), while prasinophytes contributed equally in both clusters (6%). This finding supports the observed high concentration of TChl *b*. CHEMTAX analysis showed a very low contribution of euglenophytes (3%) in the basin. Although cryptophytes contributed little to TChl *a* (6%), they dominated in the western part of the basin (stations 3-3, 3-2, and 3-7, Fig. 8) and were similar in importance to clorophytes in Cluster 1 (12%). The significant presence of cryptophytes in the western part of the basin (11%) is in agreement with the previous results of Novarino (2005), who identified 11 species in the western MS (Alboran Sea and Barcelona coasts). This finding is interesting because this group may be missed in field collections for microscopy due to their incomplete preservation.

In the picoplankton range, *Synechococcus* and *Prochlorococcus* contributed equally, with the highest values in Cluster 1 (14% for the two groups) compared to Cluster 2 (8% and 7% for *Synechococcus* and *Prochlorococcus*, respectively). The contributions in Cluster 1 are in agreement with the results of Marty et al. (2008) in the northwestern Mediterranean due to the presence of the MAW in both regions.

Diatoms had the highest contributions to TChl *a* in the AB, with values of about 14% and 22% in clusters 1 and 2, respectively. Dinoflagellates contributed less (about 12% in both clusters), but were present uniformly throughout the basin compared to diatoms, which were characterized by more patchy occurrence (Fig. 8).

Regions of high productivity with a dominance of large phytoplankton cells tend to exhibit high photosynthetic carotenoids (PSCs). In contrast, regions of low production and a dominance of small phytoplankton cells show a limited pigment diversity with an abundance of photoprotective pigments (PPCs) (Gibb et al., 2000).

The variation in community structure across the basin resulted in changes in pigment composition between the four regions. While the proportion of TChl*b* was low overall, the highest proportions were observed in the northeastern part of the basin (Fig. 9A). As shown in Fig. 9C, the increase in the proportion of TChl*b* within the total pigment pool corresponded to parallel increases in the proportions of clorophytes, *Prochlorococcus,* and, to a lesser extent, prasinophytes. In contrast, the proportion of TChl*c* was greater in the western and central regions (Fig. 9A), and this increase was mainly attributed to higher proportions of diatoms and dinoflagellates.

Similarly, the proportion of PSC was more pronounced in the central and western regions of the basin (Fig. 9A). The increase in PSC was mainly associated with increased proportions of prymnesiophytes, diatoms and dinoflagellates (Fig. 9D).

In our study, the highest PPC levels were observed in the western and central parts of the basin, which also had the highest proportions of TChl*a*. This is different from what Gibb et al. (2000) found in regions of high productivity, however, the elevated PPC proportions can be explained by the high abundance of cryptophytes in the west and *Synechococcus*, *Prochlorococcus*, and prasinophytes in the center, as shown in Fig. 8. These results confirm the observations of Barlow et al. (2004) and support our hypothesis that prasinophytes may be an additional source of ZEA, as evidenced by the increasing proportion of prasinophytes and PPC (Fig. 9E).

Table 3: Relative contributions (%) of different algal classes to chlorophyll a in Cluster 1 (Modified Atlantic Water) and Cluster 2 (Atlantic Water).

	Diatoms	*Dinoflagellates*	*Prymnesiophytes*	*Clorophytes*	*Pelagophytes*	*Prasinophytes*	*Euglenophytes*	*Cryptophytes*	*Synechococcus*	*Prochlorococcus*
Cluster 1 (MAW)	14	12	16	12	8	5	4	1	14	14
Cluster 2 (AW)	22	13	16	9	6	6	2	11	8	7

4.3. Phytoplankton vertical distribution

Our study can yield a better understanding of the vertical distribution of the phytoplankton in the AB. Except for the shallow depths in the west and the center, where the very high Chl *a* concentrations observed biased the signal, TChla/Tpig showed little variation with depth throughout the basin (Fig. 6), indicating a constant ratio of TChla/Tpig, as previously reported by Trees et al. (2000). Moreover, the west and the center of the basin were the only regions with such a shallow maximum; all other DCMs were located at greater depths. This

layer was characterized by the dominance of cryptophytes, the dominant group of the surface phytoplankton community in the west and, to a lesser extent, in the center (Fig. 7B, D). They were followed by prasinophytes, diatoms, dinoflagellates, and to a lesser extent, prymnesiophytes and *Synechococcus*, which were more prominent in Cluster 1 (Fig. 7A). This assemblage was characterized by high PPC values (Fig. 6A, B), with the main contributors being *Synechococcus* (in Cluster 1) (Fig. 7A, C) and cryptophytes, prasinophytes (in Cluster 2). The predominance of prasinophytes over *Synechococcus* (Fig. 7B) suggests that this green lineage group could be the source of the high proportion of ZEA observed in this area (34% of PPCs) (Wright et al., 1996). On the other hand, the surface layers in the east and northeast regions of the basin were dominated by prymnesiophytes, Synechococcus, and, to a lesser extent, dinoflagellates (Fig. 7E, F), explaining the ratios of surface PSC > 0.2 (Fig. 6C, D).

The observation of cryptophytes in the western part of the AB is not insignificant, since this region of the Mediterranean is known to host a high diversity of this group (Novarino, 2005). Moreover, cryptophytes are known to reach their maximum abundance in summer-autumn (Cerino and Zingone, 2006), which coincides with the sampling period of the SOMBA cruise. The occurrence of this particular assemblage at the observed depth can be attributed to two key factors. First (1) nutrient enrichment from deep waters is a likely cause, supported by correlations found between the contributions of the major groups in this layer and nutrient levels (Table 4). Second (2) cryptophytes, prymnesiophytes and dinoflagellates, known for their elevated levels of UV-absorbing compounds compared to other groups (Jeffrey et al., 1999), contributed significantly to this unique depth-related pattern.

Regarding the PSCs, high proportions were found in the DCM, where diatoms represented the major component of the phytoplankton biomass. Diatoms are known to be opportunistic species (Fogg, 1991). Their distribution followed a west-east deepening (30-100 m) and a northward decreasing trend, corresponding to the oligotrophic trend observed in the AB. The presence of diatoms in shallower layers in the west and the center (Fig. 7B, C, D) could be linked to the upwelling of nutrient-rich deep and dense waters into the surface layers. The same phenomenon was observed in the east, where the Sardinian Cyclonic Eddy induced an upwelling of nutrient-rich deep waters, leading to the proliferation of diatoms there (stations 1-2, 1-4, and 1-11) (Fig. 8). Importantly, this distribution pattern is consistent with the results of our analysis, which showed a strong correlation between the relative contribution of diatoms and nutrient levels, as shown in Table 4 and Fig. 10a. The observed correlation underscores the significant influence of nutrient availability on diatom abundance in the study area.

In contrast, the distribution of dinoflagellates was patchy and spread from surface down to 80 m. This distribution could be linked to the fact that dinoflagellates are motile and thus can accomplish vertical migrations to acquire nutrients and/or optimum photosynthetic conditions.

In addition to diatoms, other groups dominated in the deeper water column. Pelagophytes were present in the deeper depths of the entire basin and thrived below the nitracline, as evidenced by an increasing BUT/HEX ratio with depth. This could be related to nutrients, especially nitrate as controlling factor for the vertical distribution of prymnesiophytes and chrysophytes/pelagophytes (Barlow et al., 1997; Claustre et al., 1994). This is confirmed by the correlation found between pelagophytes and nitrate throughout the basin (Table 4) (Fig. 10c).

Our analysis revealed that clorophytes were a major contributor to the phytoplankton community, as evidenced by the increased proportion of TChlb/Tpig (Fig. 6D). They showed a higher abundance in Cluster 1, particularly in the northeastern part of the basin, where they dominated at the DCM.

Clorophytes, together with *Prochlorococcus,* were reponsible for the high proportions of TChl*b* observed in the basin during the cruise (Fig. 9C).

Prochlorococcus were also part of the deep phytoplankton community. In fact, the two groups of picophytoplankton showed an opposing pattern occurrence (Table 3). This pattern was also observed at the Bermuda Atlantic Time-series Study (BATS) site (DuRand et al., 2001). In our study, *Synechococcus* occupied the shallower depths of the basin with a deepening to the east and northeast (up to 90 m). They thrived below the MLD and were moderately tied to declining nutrients, as shown by the negative linear correlation between *Synechococcus* and nitrate concentration in the AB (r^2 = -0.58, rms = 0.018).

On the other hand, *Prochlorococcus* was predominant at greater depths (60-100 m), mainly within Cluster 1 (Fig. 7), which followed the nitracline. Olson et al. (1990) described the nitrate affinity of *Prochlorococcus*, as depicted in the Fig. 10b, where the contribution of *Prochlorococcus* increased with higher water density and elevated nitrate concentration. The same distribution was observed at the Hawaian Ocean Time-series station (Campbell et al., 1997), NW Mediterranean (Marty et al., 2008), and the Balearic Sea (Mena et al., 2016). The vertical abundance pattern of *Synechococcus* and *Prochlorococcus* could be attributed to the different sensitivity to light stress (Mella-Flores et al., 2012) and light adaptation of *Prochlorococcus*. Indeed, DVChl *a* and *b* of *Prochlorococcus* absorb efficiently at the wavelengths of blue light available in the deep euphotic zone (Glover et al., 1986), while *Synechococcus* absorbs blue light less efficiently (Campbell and Iturriaga, 1988; Olson

et al., 1990, 1988; Waterbury et al., 1986). Additionally, the large diversity of *Prochlorococcus* in the euphotic zone could add to its observed distribution (Garczarek et al., 2007).

Table 4: Correlation between nutrients with major phytoplankton groups: Basin-wide and DCM analyses. R^2 values are provided for all correlations, with significant values highlighted in bold.

	All data			*DCM data*		
	NO3	PO4	Si(OH)4	NO3	PO4	Si(OH)4
Pelagophytes	**0.51**	**0.46**	0.13	-	-	-
Prymnesiophyte	0.36	0.22	0.18	-	-	-
Cryptophytes	-	**0.49**	**0.50**	-	**0.48**	**0.83**
Dinoflagellates	0.29	0.24	-	-	-	-
Clorophytes	0.15	0.26	-	-	-	-
Diatoms	-	-	-	**0.44**	**0.65**	0.11
Prasinophytes	0.23	0.35	0.26	-	-	-

Fouilland et al. (2016) suggested that an increase in turbulence in the natural environment may increase phytoplankton biomass under low nutrient conditions and that eutrophic and oligotrophic conditions do not necessarily result in the dominance of diatoms and flagellates, respectively. According to Vaillancourt et al. (2003), cyclonic eddies contain cold, nutrient-rich waters associated with high phytoplankton abundance and primary production. Similar conditions were observed in the western part of the AB (Cluster 2), where the combination of the newly-entering AWs and the input of nutrient-rich, cold intermediate waters to the euphotic zone resulted in shallow nutriclines (40-50 m) and DCM (dominated by cryptophytes, prasinophytes, and prymnesiophytes), high concentrations of Chl *a* (up to 88 mg m^{-2}), a diverse phytoplankton community, and abundance of diatoms and nanoflagellates (Fig. 7). Along their eastward path, the AWs acquire Mediterranean properties and become warmer, saltier, and nutrient depleted as they go further into the AB (eastward and northward). Consequently, Cluster 1 (MAW) (which covers 60% of the basin) exhibited, as shown in this study, a typical pattern of oligotrophic regions: deep nutriclines, low phytoplankton biomass with deep DCMs, the abundance of nanoflagellates, the occurrence of *Synechococcus* in the surface layers and *Prochlorococcus* in deeper depths (60-100 m) (Fig. 7).

During the summer of 2014, Keraghel et al. (2020) found that the AB was a source of CO_2 to the atmosphere, except for its southwestern part where the basin was a CO_2 sink, suggesting high net photosynthesis, also indicated by high dissolved oxygen concentrations. Indeed, our findings support this hypothesis and show the importance of studying the phytoplankton diversity, which can lead to a better understanding of the oceanic carbon cycle.

5. Conclusion

This study represents the first comprehensive survey of phytoplankton of the entire Algerian Basin, our results indicate the dominance of prymnesiophytes (16%) and diatoms (14-22%). Prymnesiophytes showed a broad distribution throughout the water column, while diatoms thrived mainly in the deeper depths of the basin. In addition, cryptophytes were observed exclusively in the western region of the basin, and contributed about 6% to the TChl *a*. Within the picoplankton range, *Prochlorococcus* contributed about about 13% and thrived in the deep layers (60-100 m) following the nitracline. In contrast, *Synechococcus* (11%) were prevalent in shallower depths (20-60 m).

The physical-chemical characteristics of the AB influenced the composition and the relative contributions of the phytoplankton groups. In the western region, the influx of cold Atlantic waters and nutrient enrichment from below favored high production, leading to the dominance of cryptophytes, diatoms, dinoflagellates, and prymnesiophytes. Moving eastward, along the oligotrophic gradient characterized by deeper nutriclines and DCMs, the dominant groups included diatoms, *Synechococcus*, *Prochlorococcus*, clorophytes and prymnesiophytes.

We succeeded in tracing the spatial distribution of phytoplankton communities in the AB during the summer of 2014 in relation to environmental conditions from relative pigment concentrations, proving that CHEMTAX is a valuable tool for identifying and mapping phytoplankton populations and improve our understanding of the biogeochemical processes in the ocean. However, further HPLC based pigment analyses are needed to better understand the seasonal distribution of phytoplanktonic communities in the AB, especially during the winter season when the highest of Chl *a* levels are recorded.

6. Acknowledgments

The SOMBA-GE cruise was the result of an Algerian/French collaboration under the MerMex program, promoted by the I-MOOSE initiative within the framework of MISTRALS. We thank

the captains and crews of the R/V Téthys II and the scientific crew for their commitment on board. We are particularly grateful to the Laboratoire d'Océanographie de Villefranche (LOV), the Mediterranean Institute of Oceanography (MIO), for the high quality of pigment and nutrient measurements. A special thanks to Simon Wright for his precious help and advice on the CHEMTAX software.

This work was supported by the French Ministry of foreign affairs (MAEDI) under the ENVIMED program [grant number 2014, 2834-CIRMED].

References

Aiken, J., Moore, G.F., Hotligan, P.M., 1992. Remote Sensing of Oceanic Biology in Relation to Global Climate Change. Journal of Phycology 28, 579–590. https://doi.org/10.1111/j.0022-3646.1992.00579.x

Aiken, J., Pradhan, Y., Barlow, R., Lavender, S., Poulton, A., Holligan, P., Hardman-Mountford, N., 2009. Phytoplankton pigments and functional types in the Atlantic

Ocean: A decadal assessment, 1995-2005. Deep-Sea Research Part II: Topical Studies in Oceanography 56, 899–917. https://doi.org/10.1016/j.dsr2.2008.09.017

Andrie, C., Merlivat, L., 1988. Tritium in the western Mediterranean Sea during 1981 Phycemed cruise. Deep Sea Research Part A. Oceanographic Research Papers 35, 247–267. https://doi.org/10.1016/0198-0149(88)90039-8

Barlow, R., Stuart, V., Lutz, V., Sessions, H., Sathyendranath, S., Platt, T., Kyewalyanga, M., Clementson, L., Fukasawa, M., Watanabe, S., Devred, E., 2007. Seasonal pigment patterns of surface phytoplankton in the subtropical southern hemisphere. Deep Sea Research Part I: Oceanographic Research Papers 54, 1687–1703. https://doi.org/10.1016/j.dsr.2007.06.010

Barlow, R.G., Aiken, J., Moore, G., Holligan, P.M., Lavender, S., 2004. Pigment adaptations in surface phytoplankton along the eastern boundary of the Atlantic Ocean. Marine Ecology Progress Series 281, 13–26. https://doi.org/10.3354/meps281013

Barlow, R.G., Mantoura, R.F.C., Cummings, D.G., Fileman, T.W., 1997. Pigment chemotaxonomic distributions of phytoplankton during summer in the western Mediterranean. Deep-Sea Research Part II: Topical Studies in Oceanography 44, 833–850. https://doi.org/10.1016/S0967-0645(96)00089-6

Barlow, R.G., Mantoura, R.F.C., Gough, M.A., Fileman, T.W., 1993. Pigment signatures of the phytoplankton composition in the northeastern Atlantic during the 1990 spring bloom. Deep Sea Research Part II: Topical Studies in Oceanography 40, 459–477. https://doi.org/10.1016/0967-0645(93)90027-K

Benzouaï, S., Louanchi, F., Smara, Y., 2020. Phytoplankton phenology in algerian continental shelf and slope waters using remotely sensed data. Estuarine, Coastal and Shelf Science 247, 107070. https://doi.org/10.1016/j.ecss.2020.107070

Bethoux, J., 1980. Mean water fluxes across sections in the mediterranean-sea, evaluated on the basis of water and salt budgets and of observed salinities. Oceanologica Acta 3, 79–88.

Broecker, W.S., Peng, T.-H., 1982. Tracers in the Sea, Lamont-Doherty Geological observatory, Columbia university. ed. New York.

Brunet, C., Casotti, R., Aronne, B., Vantrepotte, V., 2003. Measured photophysiological parameters used as tools to estimate vertical water movements in the coastal Mediterranean. Journal of Plankton Research 25, 1413–1425. https://doi.org/10.1093/plankt/fbg091

Bustillos-Guzman, J., Claustre, H., Marty, J.C., 1995. Specific phytoplankton signatures and their relationship to hydrographic conditions in the coastal northwestern

Mediterranean Sea. Marine Ecology Progress Series 124, 247–258. https://doi.org/10.3354/meps124247

Campbell, L., Iturriaga, R., 1988. Identification of Synechococcus spp. in the Sargasso Sea by Immunofluorescence and Fluorescence Excitation Spectroscopy Performed on Individual Cells. Limnology and Oceanography 33, 1196–1201.

Campbell, L., Liu, H., Nolla, H.A., Vaulot, D., 1997. Annual variability of phytoplankton and bacteria in the subtropical North Pacific Ocean at Station ALOHA during the 1991–1994 ENSO event. Deep Sea Research Part I: Oceanographic Research Papers 44, 167–192. https://doi.org/10.1016/S0967-0637(96)00102-1

Cerino, F., Zingone, A., 2006. A survey of cryptomonad diversity and seasonality at a coastal Mediterranean site. European Journal of Phycology 41, 363–378. https://doi.org/10.1080/09670260600839450

Chris, S., Feely, R., 2007. The oceanic sink for carbon dioxide. Greenhouse Gas Sinks 31–49. https://doi.org/10.1079/9781845931896.0031

Claustre, H., Kerherve, P., Marty, J.C., Prieur, L., Videau, C., Hecq, J.H., 1994. Phytoplankton dynamics associated with a geostrophic front: Ecological and biogeochemical implications. J.Mar.Res. 52, 711–742. https://doi.org/10.1357/0022240943077000

Claustre, H., Marty, J.C., 1995. Specific phytoplankton biomasses and their relation to primary production in the tropical North Atlantic. Deep-Sea Research Part I 42, 1475–1493. https://doi.org/10.1016/0967-0637(95)00053-9

Cotroneo, Y., Aulicino, G., Ruiz, S., Pascual, A., Budillon, G., Fusco, G., Tintoré, J., 2016. Glider and satellite high resolution monitoring of a mesoscale eddy in the algerian basin: Effects on the mixed layer depth and biochemistry. Journal of Marine Systems 162, 73–88. https://doi.org/10.1016/j.jmarsys.2015.12.004

Crispi, G., Mosetti, R., Solidoro, C., Crise, A., 2001. Nutrients cycling in Mediterranean basins: the role of the biological pump in the trophic regime. Ecological Modelling 138, 101–114. https://doi.org/10.1016/S0304-3800(00)00396-3

D'Ortenzio, F., Ribera d'Alcalà, M., 2009. On the trophic regimes of the Mediterranean Sea: a satellite analysis. Biogeosciences 6, 139–148. https://doi.org/10.5194/bg-6-139-2009

DuRand, M.D., Olson, R.J., Chisholm, S.W., 2001. Phytoplankton population dynamics at the Bermuda Atlantic Time-series station in the Sargasso Sea. Deep Sea Research Part II: Topical Studies in Oceanography 48, 1983–2003. https://doi.org/10.1016/S0967-0645(00)00166-1

Durrieu de Madron, X., Guieu, C., Sempéré, R., Conan, P., Cossa, D., D'Ortenzio, F., Estournel, C., 2011. Marine ecosystems' responses to climatic and anthropogenic forcings in the Mediterranean.

Everitt, D.A., Wright, S.W., Volkman, J.K., Thomas, D.P., Lindstrom, E.J., 1990. Phytoplankton community compositions in the western equatorial Pacific determined from chlorophyll and carotenoid pigment distributions. Deep Sea Research Part A. Oceanographic Research Papers 37, 975–997. https://doi.org/10.1016/0198-0149(90)90106-6

Fogg, G.E., 1991. Changing Productivity of the Oceans in Response to a Changing Climate. Annals of Botany 67, 57–60.

Font, J., Isern-Fontanet, J., Salas, J.D.J., 2004. Tracking a big anticyclonic eddy in the western Mediterranean Sea. Scientia Marina 68, 331–342. https://doi.org/10.3989/scimar.2004.68n3331

Fouilland, E., Mostajir, B., Gosselin, M., Levasseur, M., Roy, S., Vidussi, F., De Mora, S., Demers, S., 2016. Effect of mixing on the structure of a natural plankton community: A mesocosm study. Vie et Milieu 66, 251–259.

Fuda, J.L., Millot, C., Taupier-Letage, I., Send, U., Bocognano, J.M., 2000. XBT monitoring of a meridian section across the western Mediterranean Sea. Deep Sea Research Part I: Oceanographic Research Papers 47, 2191–2218. https://doi.org/10.1016/S0967-0637(00)00018-2

Garczarek, L., Dufresne, A., Rousvoal, S., West, N.J., Mazard, S., Marie, D., Claustre, H., Raimbault, P., Post, A.F., Scanlan, D.J., Partensky, F., 2007. High vertical and low horizontal diversity of Prochlorococcus ecotypes in the Mediterranean Sea in summer. FEMS microbiology ecology 60, 189–206. https://doi.org/10.1111/j.1574-6941.2007.00297.x

Gibb, S.W., Barlow, R.G., Cummings, D.G., Rees, N.W., Trees, C.C., Holligan, P., Suggett, D., 2000. Surface phytoplankton pigment distributions in the Atlantic Ocean: An assessment of basin scale variability between 50°N and 50°S. Progress in Oceanography 45, 339–368. https://doi.org/10.1016/S0079-6611(00)00007-0

Gibb, S.W., Cummings, D.G., Irigoien, X., Barlow, R.G., Fauzi, R., Mantoura, C., 2001. Phytoplankton pigment chemotaxonomy of the northeastern Atlantic. Deep-Sea Research Part II: Topical Studies in Oceanography 48, 795–823. https://doi.org/10.1016/S0967-0645(00)00098-9

Gieskes, W.W., Kraay, G.W., 1986. Floristic and physiological differences between the shallow and the deep nanophytoplankton community in the euphotic zone of the open

tropical Atlantic revealed by HPLC analysis of pigments. Marine Biology 91, 567–576. https://doi.org/10.1007/BF00392609

Glover, H.E., Keller, M.D., Guillard, R.R.L., 1986. Light quality and oceanic ultraphytoplankters. Nature 319, 142–143. https://doi.org/10.1038/319142a0

Harid, R., Demarcq, H., Keraghel, M.-A., Ait-Kaci, M., Zerrouki, M., Bachari, N.-E.-I., Houma, F., 2022. Spatio-temporal variability of a chlorophyll-a based biomass index and influence of coastal sources of enrichment in the Algerian Basin. Continental Shelf Research 232, 104629. https://doi.org/10.1016/j.csr.2021.104629

Higgins, H.W., Wright, S.W., Schlüter, L., 2011. Quantitative interpretation of chemotaxonomic pigment data, in: Llewellyn, C.A., Egeland, E.S., Johnsen, G., Roy, S. (Eds.), Phytoplankton Pigments: Characterization, Chemotaxonomy and Applications in Oceanography, Cambridge Environmental Chemistry Series. Cambridge University Press, Cambridge, pp. 257–313.

Hou, J.-J., Huang, B.-Q., Cao, Z.-R., Chen, J.-X., Hong, H.-S., 2007. Effects of Nutrient Limitation on Pigments in Thalassiosira weissflogii and Prorocentrum donghaiense. Journal of Integrative Plant Biology 49, 686–697. https://doi.org/10.1111/j.1744-7909.2007.00449.x

Ignatiades, L., 2005. Scaling the trophic status of the Aegean Sea, eastern Mediterranean. Journal of Sea Research, Contrasting Approaches to Understanding Eutrophication Effects on Phytoplankton 54, 51–57. https://doi.org/10.1016/j.seares.2005.02.010

Illoul, H., Masó, M., Fortuño, J.-M., Cros, L., Morales-Blake, A., Séridji, R., 2008. Potentially harmful microalgae in coastal waters of the Algiers area (Southern Mediterranean Sea) 18.

Jeffrey, S., Vesk, M., 1997. Introduction to marine phytoplankton and their pigment signatures. Phytoplankton pigments in oceanography-Guidelines to modern methods 37–84.

Jeffrey, S.W., MacTavish, H.S., Dunlap, W.C., Vesk, M., Groenewoud, K., 1999. Occurrence of UVA- and UVB-absorbing compounds in 152 species (206 strains) of marine microalgae. Marine Ecology Progress Series 189, 35–51.

Keraghel, M.A., Louanchi, F., Zerrouki, M., Aït Kaci, M., Aït-Ameur, N., Labaste, M., Legoff, H., Taillandier, V., Harid, R., Mortier, L., 2020. Carbonate system properties and anthropogenic carbon inventory in the Algerian Basin during SOMBA cruise (2014): Acidification estimate. Marine Chemistry 221. https://doi.org/10.1016/j.marchem.2020.103783

Kheireddine, M., Ouhssain, M., Claustre, H., Uitz, J., Gentili, B., Jones, B.H., 2017. Assessing Pigment-Based Phytoplankton Community Distributions in the Red Sea. Frontiers in Marine Science 4.

Kirk, J.T.O., 1994. Light and Photosynthesis in Aquatic Ecosystems. Cambridge Core.

Kress, N., Herut, B., 2001. Spatial and seasonal evolution of dissolved oxygen and nutrients in the Southern Levantine Basin (Eastern Mediterranean Sea): Chemical characterization of the water masses and inferences on the N : P ratios. Deep-Sea Research Part I: Oceanographic Research Papers 48, 2347–2372. https://doi.org/10.1016/S0967-0637(01)00022-X

Krom, M.D., Kress, N., Brenner, S., Gordon, L.I., 1991. Phosphorus limitation of primary productivity in the eastern Mediterranean Sea. Limnology and Oceanography 36, 424–432. https://doi.org/10.4319/lo.1991.36.3.0424

Langdon, C., 2010. Determination of Dissolved Oxygen in Seawater by Winkler Titration Using The Amperometric Technique. https://doi.org/10.25607/OBP-1350

Latasa, M., 2007. Improving estimations of phytoplankton class abundances using CHEMTAX. Marine Ecology-progress Series - MAR ECOL-PROGR SER 329, 13–21. https://doi.org/10.3354/meps329013

Ludwig, W., Bouwman, A.F., Dumont, E., Lespinas, F., 2010. Water and nutrient fluxes from major Mediterranean and Black Sea rivers: Past and future trends and their implications for the basin-scale budgets. Global Biogeochemical Cycles 24. https://doi.org/10.1029/2009GB003594

Mackey, M.D., Mackey, D.J., Higgins, H.W., Wright, S.W., 1996. CHEMTAX - A program for estimating class abundances from chemical markers: Application to HPLC measurements of phytoplankton. Marine Ecology Progress Series 144, 265–283. https://doi.org/10.3354/meps144265

Mallil, K., Testor, P., Bosse, A., Margirier, F., Houpert, L., Herve, L.G., Mortier, L., Louanchi, F., 2022. The Levantine Intermediate Water in the western Mediterranean and its interactions with the Algerian Gyres: insights from 60 years of observation. Ocean Science 18, 937–952. https://doi.org/10.5194/os-18-937-2022

Marty, J.C., Garcia, N., Raimbault, P., 2008. Phytoplankton dynamics and primary production under late summer conditions in the NW Mediterranean Sea. Deep-Sea Research Part I: Oceanographic Research Papers 55, 1131–1149. https://doi.org/10.1016/j.dsr.2008.05.001

Mella-Flores, D., Six, C., Ratin, M., Partensky, F., Boutte, C., Gildas, L.C., Marie, D., Blot, N., Gourvil, P., Kolowrat, C., Garczarek, L., 2012. Prochlorococcus and

Synechococcus have evolved different adaptive mechanisms to cope with light and UV stress. Frontiers in Microbiology 3, 285. https://doi.org/10.3389/fmicb.2012.00285

Mena, C., Reglero, P., Ferriol, P., Torres, A., Aparicio-González, A., Balbín, R., Santiago, R., Moyà, G., Alemany, F., Agawin, N.S., 2016. Prokaryotic picoplankton spatial distribution during summer in a haline front in the Balearic Sea, Western Mediterranean. Hydrobiologia 779. https://doi.org/10.1007/s10750-016-2825-4

Mignot, A., Claustre, H., Uitz, J., Poteau, A., D'Ortenzio, F., Xing, X., 2014. Understanding the seasonal dynamics of phytoplankton biomass and the deep chlorophyll maximum in oligotrophic environments: A Bio-Argo float investigation. Global Biogeochemical Cycles. https://doi.org/10.1002/2013GB004781

Millot, C., 1999. Circulation in the Western Mediterranean Sea. Journal of Marine Systems 20, 423–442. https://doi.org/10.1016/S0924-7963(98)00078-5

Millot, C., 1987. Circulation in the western mediterranean-sea. Oceanologica Acta 10, 143–149.

Millot, C., 1985. Some features of the Algerian Current. Journal of Geophysical Research: Oceans 90, 7169–7176. https://doi.org/10.1029/JC090iC04p07169

Millot, C., Taupier-Letage, I., 2005. Circulation in the Mediterranean Sea, in: Saliot, A. (Ed.), The Mediterranean Sea, Handbook of Environmental Chemistry. Springer, Berlin, Heidelberg, pp. 29–66.

Miranda-Alvarez, C., González-Silvera, A., Santamaría-del-Angel, E., López-Calderón, J., Godínez, V.M., Sánchez-Velasco, L., Hernández-Walls, R., 2020. Phytoplankton pigments and community structure in the northeastern tropical pacific using HPLC-CHEMTAX analysis. Journal of Oceanography 76, 91–108. https://doi.org/10.1007/s10872-019-00528-3

Morán, X.A.G., Taupier-Letage, I., Vázquez-Domínguez, E., Ruiz, S., Arin, L., Raimbault, P., Estrada, M., 2001. Physical-biological coupling in the Algerian basin (SW Mediterranean): Influence of mesoscale instabilities on the biomass and production of phytoplankton and bacterioplankton. Deep-Sea Research Part I: Oceanographic Research Papers 48, 405–437. https://doi.org/10.1016/S0967-0637(00)00042-X

Moutin, T., Prieur, L., 2012. Influence of anticyclonic eddies on the Biogeochemistry from the Oligotrophic to the Ultraoligotrophic Mediterranean (BOUM cruise). Biogeosciences 9, 3827–3855. https://doi.org/10.5194/bg-9-3827-2012

Mustapha, B., 2021. Characterization of the ecosystem and the status of phytoplankton populations in the Alboran Sea and the Algerian Basin from 2013 to 2015 during the

spring season. Marine Biodiversity 12, 855–863. https://doi.org/10.31396/Biodiv.Jour.2021.12.4.855.863

Novarino, G., 2005. Nanoplankton protists from the western Mediterranean Sea. II. Cryptomonads (Cryptophyceae = Crptomonadea). Scientia Marina 69. https://doi.org/10.3989/scimar.2005.69n147

Olita, A., Ribotti, A., Sorgente, R., Fazioli, L., Perilli, A., 2010. SLA–chlorophyll-a variability and covariability in the Algero-Provençal Basin (1997–2007) through combined use of EOF and wavelet analysis of satellite data. Ocean Dynamics 2010 61:1 61, 89–102. https://doi.org/10.1007/S10236-010-0344-9

Olson, R.J., Chisholm, S.W., Zettler, E.R., Altabet, M.A., Dusenberry, J.A., 1990. Spatial and temporal distributions of prochlorophyte picoplankton in the North Atlantic Ocean. Deep Sea Research Part A. Oceanographic Research Papers 37, 1033–1051. https://doi.org/10.1016/0198-0149(90)90109-9

Olson, R.J., Chisholm, S.W., Zettler, E.R., Armbrust, E.V., 1988. Analysis of Synechococcus pigment types in the sea using single and dual beam flow cytometry. Deep Sea Research Part A. Oceanographic Research Papers 35, 425–440. https://doi.org/10.1016/0198-0149(88)90019-2

Ondrusek, M.E., Bidigare, R.R., Sweet, S.T., Defreitas, D.A., Brooks, J.M., 1991. Distribution of phytoplankton pigments in the North Pacific Ocean in relation to physical and optical variability. Deep Sea Research Part A. Oceanographic Research Papers 38, 243–266. https://doi.org/10.1016/0198-0149(91)90082-Q

Pasqueron de Fommervault, O., Migon, C., D'Ortenzio, F., Ribera d'Alcalà, M., Coppola, L., 2015. Temporal variability of nutrient concentrations in the northwestern Mediterranean sea (DYFAMED time-series station). Deep-Sea Research Part I: Oceanographic Research Papers 100, 1–12. https://doi.org/10.1016/j.dsr.2015.02.006

Puillat, I., Taupier-Letage, I., Millot, C., 2002. Algerian Eddies lifetime can near 3 years. Journal of Marine Systems 31, 245–259. https://doi.org/10.1016/S0924-7963(01)00056-2

Pujo-Pay, M., Conan, P., Oriol, L., Cornet-Barthaux, V., Falco, C., Ghiglione, J.-F., Goyet, C., Moutin, T., Prieur, L., 2011. Integrated survey of elemental stoichiometry (C, N, P) from the western to eastern Mediterranean Sea. Biogeosciences 8, 883–899. https://doi.org/10.5194/bg-8-883-2011

Raimbault, P., Coste, B., Boulhadid, M., Boudjellal, B., 1993. Origin of high phytoplankton concentration in deep chlorophyll maximum (DCM) in a frontal region of the

Southwestern Mediterranean Sea (algerian current). Deep Sea Research Part I: Oceanographic Research Papers 40, 791–804. https://doi.org/10.1016/0967-0637(93)90072-B

Ras, J., Claustre, H., Uitz, J., 2008. Spatial variability of phytoplankton pigment distributions in the Subtropical South Pacific Ocean: comparison between in situ and predicted data. Biogeosciences 5, 353–369. https://doi.org/10.5194/bg-5-353-2008

Rodríguez, F., Chauton, M., Johnsen, G., Andresen, K., Olsen, L., M, Z., 2006. Photoacclimation in phytoplankton: Implications for biomass estimates, pigment functionality and chemotaxonomy. Marine Biology 148, 963–971. https://doi.org/10.1007/s00227-005-0138-7

Sabine, C.L., Feely, R.A., Gruber, N., Key, R.M., Lee, K., Bullister, J.L., Wanninkhof, R., Wong, C.S., Wallace, D.W.R., Tilbrook, B., Millero, F.J., Peng, T.-H., Kozyr, A., Ono, T., Rios, A.F., 2004. The Oceanic Sink for Anthropogenic CO2. Science 305, 367–371. https://doi.org/10.1126/science.1097403

Schlitzer, Reiner, Ocean Data View, https://odv.awi.de, 2021.

Schlüter, L., Møhlenberg, F., Havskum, H., Larsen, S., 2000. The use of phytoplankton pigments for identifying and quantifying phytoplankton groups in coastal areas: testing the influence of light and nutrients on pigment/chlorophyll a ratios. Marine Ecology Progress Series 192, 49–63.

Schroeder, K., Gasparini, G.P., Borghini, M., Cerrati, G., Delfanti, R., 2010. Biogeochemical tracers and fluxes in the Western Mediterranean Sea, spring 2005. Journal of Marine Systems 80, 8–24. https://doi.org/10.1016/j.jmarsys.2009.08.002

Staehr, P., Markager, S., Sand-Jensen, K., 2004. Pigment specific in vivo light absorption of phytoplankton from estuarine, coastal and oceanic waters. Marine Ecology-progress Series - MAR ECOL-PROGR SER 275, 115–128. https://doi.org/10.3354/meps275115

Tanhua, T., Hainbucher, D., Schroeder, K., Cardin, V., Álvarez, M., Civitarese, G., 2013. The Mediterranean Sea system: a review and an introduction to the special issue. Ocean Science 9, 789–803. https://doi.org/10.5194/os-9-789-2013

Taupier-Letage, I., Puillat, I., Millot, C., Raimbault, P., 2003. Biological response to mesoscale eddies in the Algerian Basin. Journal of Geophysical Research. Oceans 108. https://doi.org/10.1029/1999JC000117

Testor, P., Gascard, J.-C., 2005. Large scale flow separation and mesoscale eddy formation in the Algerian Basin. Progress In Oceanography 211–230. https://doi.org/10.1016/j.pocean.2004.07.018

Thingstad, T.F., Krom, M., Mantoura, R., Flaten, G.A., Groom, S., Herut, B., Kress, N., Law, C., Pasternak, A., Pitta, P., Psarra, S., Rassoulzadegan, F., Tanaka, T., Tselepides, A., Wassmann, P., Woodward, E., Riser, C., Zodiatis, G., Zohary, T., 2005. Nature of Phosphorus Limitation in the Ultraoligotrophic Eastern Mediterranean. Science (New York, N.Y.) 309, 1068–71. https://doi.org/10.1126/science.1112632

Thompson, P.A., Pesant, S., Waite, A.M., 2007. Contrasting the vertical differences in the phytoplankton biology of a dipole pair of eddies in the south-eastern Indian Ocean. Deep Sea Research Part II: Topical Studies in Oceanography, The Leeuwin Current and its Eddies 54, 1003–1028. https://doi.org/10.1016/j.dsr2.2006.12.009

Trees, C.C., Clark, D.K., Bidigare, R.R., Ondrusek, M.E., Mueller, J.L., 2000. Accessory pigments versus chlorophyll a concentrations within the euphotic zone: A ubiquitous relationship. Limnol. Oceanogr 45, 1130–1143.

Tréguer, P., Le Corre, P., 1975. Manuel d'analyse des sels nutritifs dans l'eau de mer (utilisation de l'autoanalyzer II Technicon R). UBO, Brest, France.

Vaillancourt, R.D., Marra, J., Seki, M.P., Parsons, M.L., Bidigare, R.R., 2003. Impact of a cyclonic eddy on phytoplankton community structure and photosynthetic competency in the subtropical North Pacific Ocean ARTICLE IN PRESS. Deep-Sea Research I 50, 829–847. https://doi.org/10.1016/S0967-0637(03)00059-1

Vidussi, F., Claustre, H., Manca, B.B., Luchetta, A., Marty, J.-C., 2001. Phytoplankton pigment distribution in relation to upper thermocline circulation in the eastern Mediterranean Sea during winter. Journal of Geophysical Research: Oceans 106, 19939–19956. https://doi.org/10.1029/1999JC000308

Waterbury, J., Watson, S., Valois, F., Franks, D., 1986. Biological and ecological characterization of the marine unicellular cyanobacterium Synechococcus, in: Photosynthetic Picoplankton. pp. 71-.

Wood, A.M., 1985. Adaptation of photosynthetic apparatus of marine ultraphytoplankton to natural light fields. Nature 316, 253–255. https://doi.org/10.1038/316253a0

Wright, S.W., Ishikawa, A., Marchant, H.J., Davidson, A.T., Van Den Enden, R.L., Nash, G.V., 2009. Composition and significance of picophytoplankton in Antarctic waters. Polar Biology 32, 797–808. https://doi.org/10.1007/s00300-009-0582-9

Wright, S.W., Thomas, D.P., Marchant, H.J., Higgins, H.W., Mackey, M.D., Mackey, D.J., 1996. Analysis of phytoplankton of the Australian sector of the Southern Ocean: Comparisons of microscopy and size frequency data with interpretations of pigment HPLC data using the "CHEMTAX" matrix factorisation program. Marine Ecology Progress Series 144, 285–298. https://doi.org/10.3354/meps144285

Liste of Figures:

Fig. 1. *Track of the SOMBA cruise with stations sampled for pigments (dark dots) and stations without pigments (red dots) superimposed on the mean sea level anomaly (m) (SLA) map showing the instabilities found during the cruise time period. 1 and 2 represent the west-east (WE) and the east-northeast (ENE) transects, respectively. Figures were produced using Ocean Data View software (Schlitzer, 2021).*

Fig. 2. *Stations of Cluster 1 (MAW) and Cluster 2 (AW) superimposed on mean sea surface salinity map during the SOMBA cruise.*

Fig. 3. *Vertical distribution of temperature* ***(A)****, potential density anomaly* ***(B)*** *(with MLD in dashed lines), concentrations of nitrate* ***(C)****, phosphate* ***(D)****, and silicate* ***(E)****, represented on the two transects WE (WE Stations) and ENE (ENE Stations) during the SOMBA cruise.*

Fig. 4. *Scatter plot of the N:P ratio distribution in the AB over the first 120 m during the SOMBA cruise.*

Fig. 5. *Vertical distribution of total chlorophyll a* ***(TChl a)****, 19'-hexanoyloxyfucoxanthin* ***(HEX)****, fucoxanthin* ***(FUCO)****, zeaxanthin* ***(ZEA)****, divinyl-chlorophyll a* ***(DVChl a)****, represented on the WE transect (WE Stations) and ENE transect (ENE Stations). Major and minor pigments are illustrated separately, with a similar scale for each.*

Fig. 6. *Vertical distribution of photo-pigment indices in the west (a), central (b), east (c), and northeast (d) regions of the AB.*

Fig. 7. *Vertical distribution of phytoplankton groups' biomass (as TChl a concentration derived from CHEMTAX using pigment concentrations with depth) in representative regions of the AB: WEST (Cluster 1)* ***(A)****, WEST (Cluster 2)* ***(B)****, CENTER (Cluster 1)* ***(C)****, CENTER (Cluster 2)* ***(D)****, NORTHEAST* ***(E)****, and EAST* ***(F)****. Note the different scales.*

Fig. 8. *Variation of phytoplankton groups (relative percent contributions to TChl a) derived from CHEMTAX using pigments' integrated concentrations in representative regions:* ***WC1*** *(west Cluster 1),* ***WC2*** *(west Cluster 2),* ***CC1*** *(center Cluster 1),* ***CC2*** *(center Cluster 2),* ***E*** *(east) and* ***NE*** *(northeast) of the Algerian basin.*

Fig. 9. *Photo-pigment indices for the four regions of the AB and relationships between selected photo-pigment indices and selected phytoplankton group proportions. TChlb: total chlorophyll b; TChlc: total chlorophyll c; PSC: photosynthetic carotenoids; PPC: photoprotective carotenoids.*

Fig. 10. *Relationship between the abundances of Diatoms (a), Prochlorococcus (b), and Pelagophytes (c) with nitrate concentration during the SOMBA cruise.*

Table 1: Ratio matrices used in CHEMTAX analysis: a) initial ratios before analysis, b) optimized ratios after analysis (Cluster 1), c) optimized ratios after analysis (Cluster 2).

Marker pigments	PERI	BUT	FUCO	HEX	NEOX	PRAS	VIOL	DDX	ALLO	ZEA	DVChl *b*	Chl*b*	DVChl *a*	Chl *a*
Class														
(a) Initial Ratio matrix														
Synechococcus	0	0	0	0	0	0	0	0	0	0.636	0	0	0	1
Prochlorococcus	0	0	0	0	0	0	0	0	0	0.321	1.074	0	1	0
Diatoms	0	0	0.623	0	0	0	0	0.163	0	0	0	0	0	1
Pelagophytes	0	0.658	0.779	0	0	0	0	0.191	0	0	0	0	0	1
Prymnesiophytes	0	0	0	1.708	0	0	0	0.101	0	0	0	0	0	1
Cryptophytes	0	0	0	0	0	0	0	0	0.379	0	0	0	0	1
Dinoflagellates	0.558	0	0	0	0	0	0	0.253	0	0	0	0	0	1
Euglenophytes	0	0	0	0	0.068	0	0	0.251	0	0	0	0.377	0	1
Clorophytes	0	0	0	0	0.066	0	0.049	0	0	0.032	0	0.315	0	1
Prasinophytes	0	0	0	0	0.063	0.245	0.054	0	0	0	0	0.704	0	1
(b) Final Ratio matrix (Cluster 1)														
Synechococcus	0	0	0	0	0	0	0	0	0	0.594	0	0	0	1
Prochlorococcus	0	0	0	0	0	0	0	0	0	0.252	0.959	1	1	0
Diatoms	0	0	0.634	0	0	0	0	0.021	0	0	0	0	0	1
Pelagophytes	0	1.158	0.509	0	0	0	0	0.039	0	0	0	0	0	1

Prymnesiophytes	0	0	0	1.155	0	0	0	0.069	0	0	0	0	0	1
Cryptophytes	0	0	0	0	0	0	0	0	0.278	0	0	0	0	1
Dinoflagellates	0.677	0	0	0	0	0	0	0.119	0	0	0	0	0	1
Euglenophytes	0	0	0	0	0.028	0	0	0.436	0	0	0	0.39	0	1
Clorophytes	0	0	0	0	0.056	0	0.019	0	0	0.049	0	0.502	0	1
Prasinophytes	0	0	0	0	0.099	0.257	0.074	0	0	0	0	0.575	0	1
(c) Final Ratio matrix (Cluster 2)														
Synechococcus	0	0	0	0	0	0	0	0	0	0.526	0	0	0	1
Prochlorococcus	0	0	0	0	0	0	0	0	0	0.439	0.121	0	1	0
Diatoms	0	0	0.605	0	0	0	0	0.035	0	0	0	0	0	1
Pelagophytes	0	1.833	0.473	0	0	0	0	0.043	0	0	0	0	0	1
Prymnesiophytes	0	0	0	1.424	0	0	0	0.062	0	0	0	0	0	1
Cryptophytes	0	0	0	0	0	0	0	0	0.278	0	0	0	0	1
Dinoflagellates	0.603	0	0	0	0	0	0	0.102	0	0	0	0	0	1
Euglenophytes	0	0	0	0	0.024	0	0	0.462	0	0	0	0.334	0	1
Clorophytes	0	0	0	0	0.063	0	0.023	0	0	0.023	0	0.583	0	1
Prasinophytes	0	0	0	0	0.11	0.285	0.08	0	0	0	0	0.624	0	1

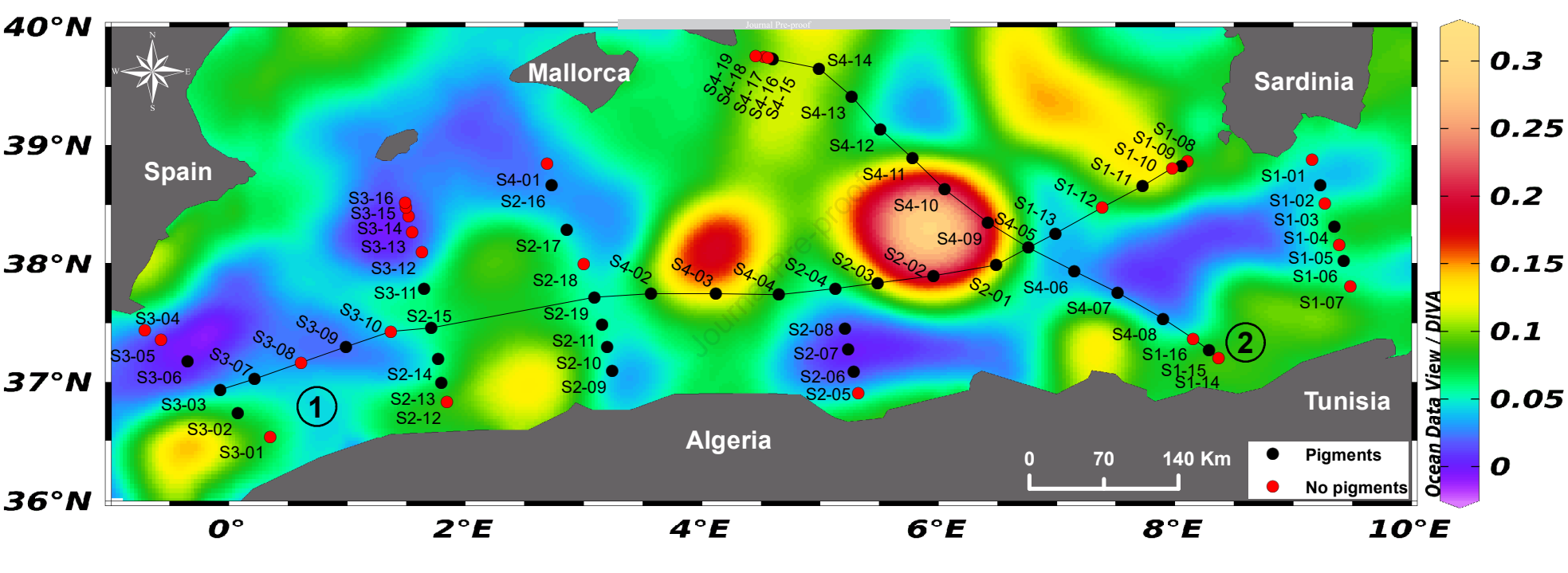
Journal Pre-proof
40°N
39°N
38°N
37°N
36°N
0°
2°E
4°E
6°E
8°E
10°E
Spain
Mallorca
Sardinia
Algeria
Tunisia
S4-19
S4-18
S4-17
S4-16
S4-15
S4-14
S4-13
S4-12
S4-11
S4-10
S4-09
S4-08
S4-07
S4-06
S4-05
S4-04
S4-03
S4-02
S4-01
S3-16
S3-15
S3-14
S3-13
S3-12
S3-11
S3-10
S3-09
S3-08
S3-07
S3-06
S3-05
S3-04
S3-03
S3-02
S3-01
S2-17
S2-16
S2-18
S2-19
S2-15
S2-14
S2-13
S2-12
S2-11
S2-10
S2-09
S2-08
S2-07
S2-06
S2-05
S2-04
S2-03
S2-02
S2-01
S1-08
S1-09
S1-10
S1-11
S1-12
S1-13
S1-01
S1-02
S1-03
S1-04
S1-05
S1-06
S1-07
S1-16
S1-15
S1-14
1
2
0
70
140 Km
Pigments
No pigments
Ocean Data View / DIVA
0.3
0.25
0.2
0.15
0.1
0.05
0

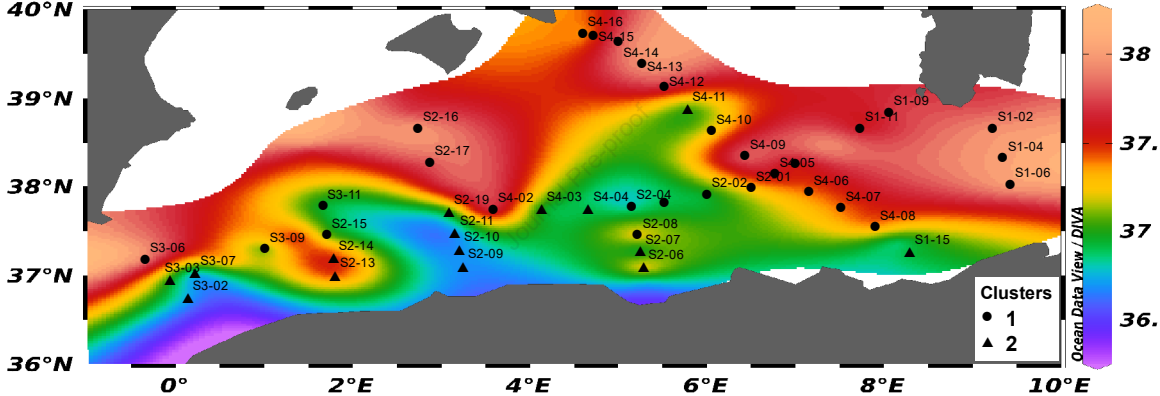

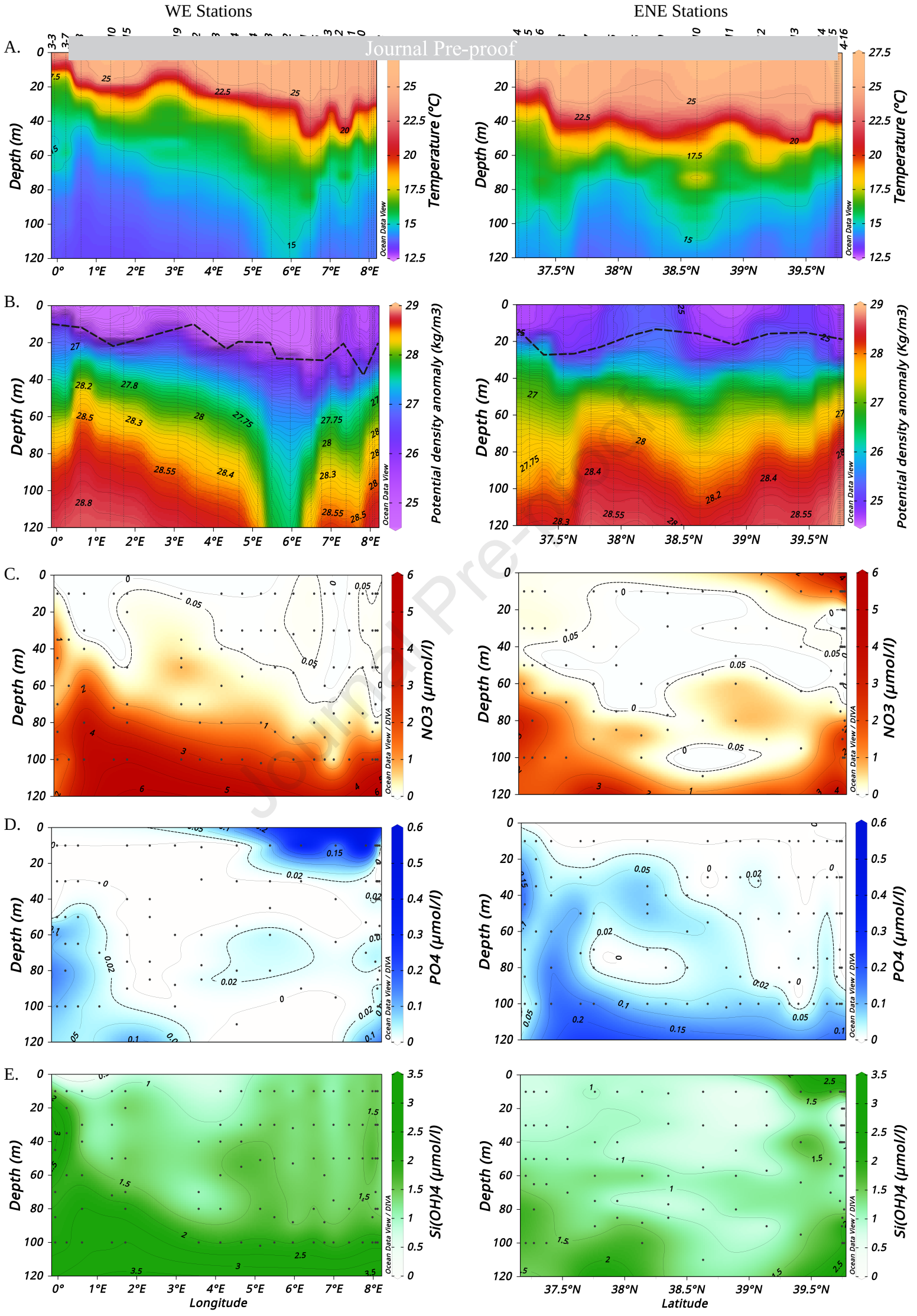

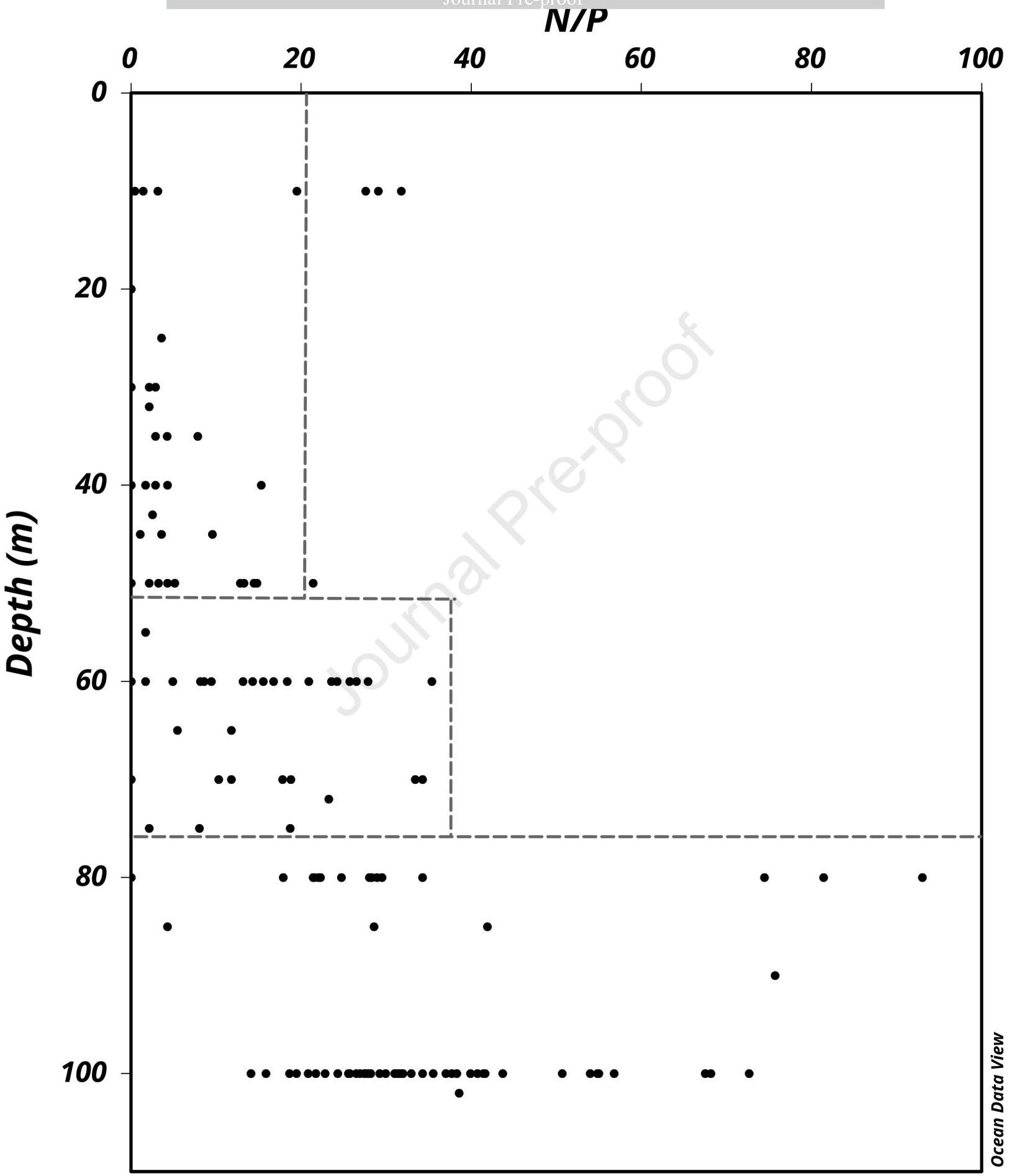

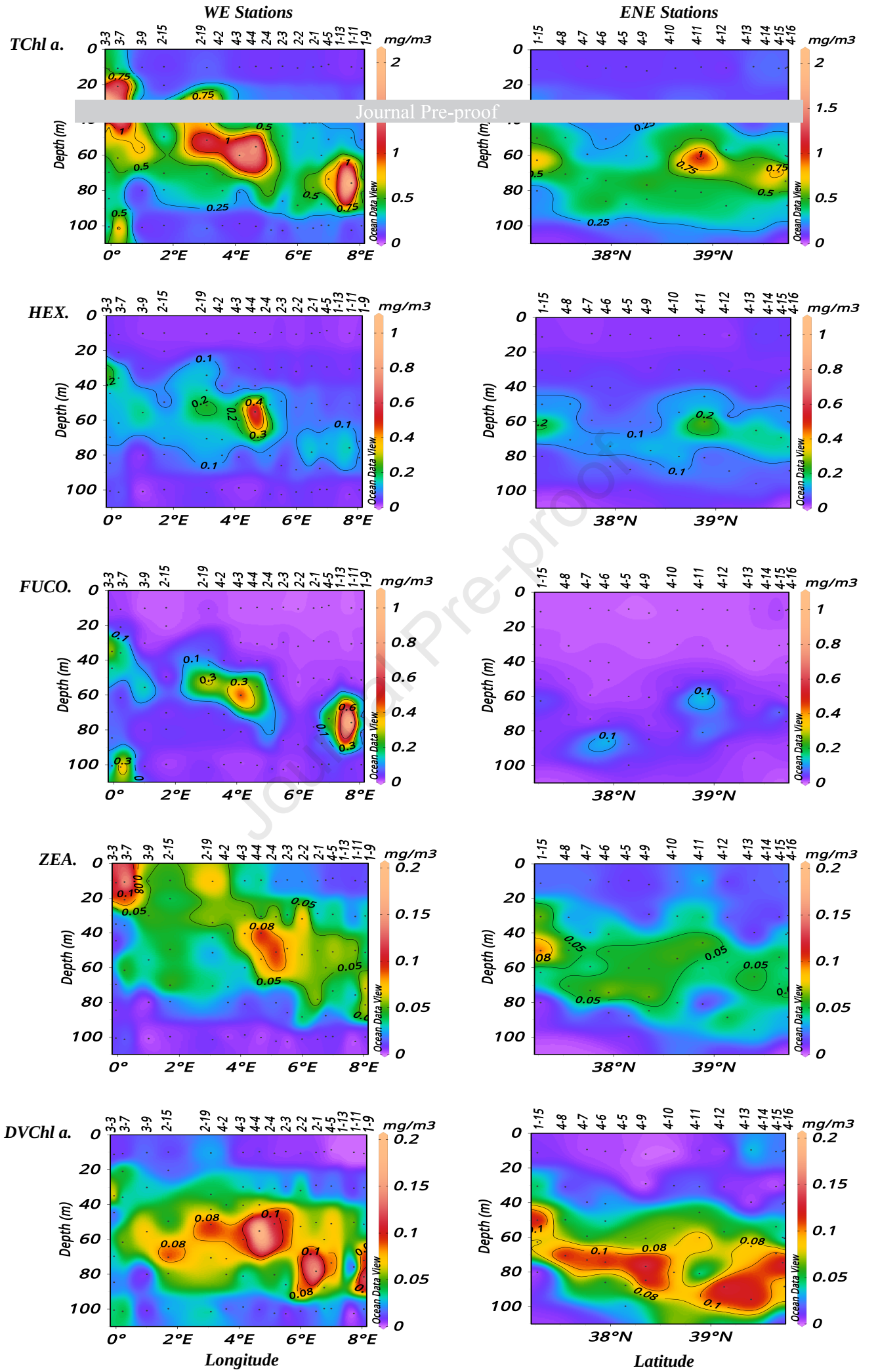

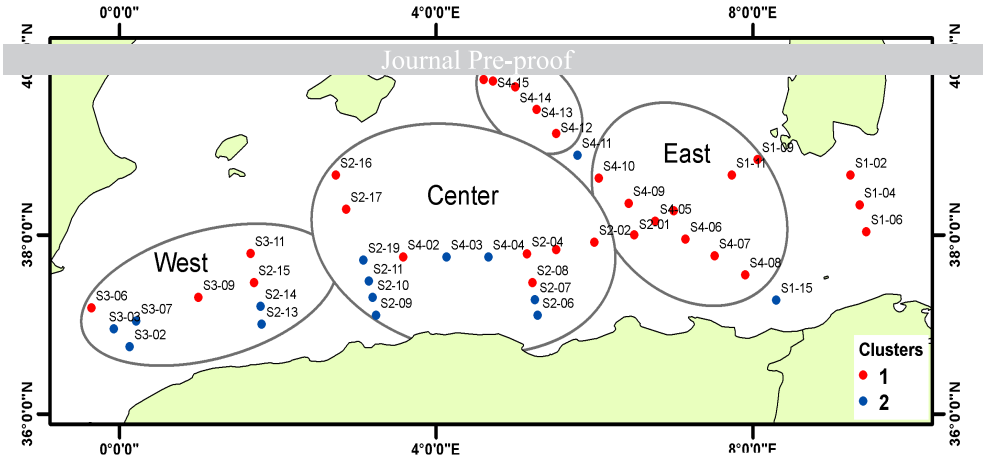

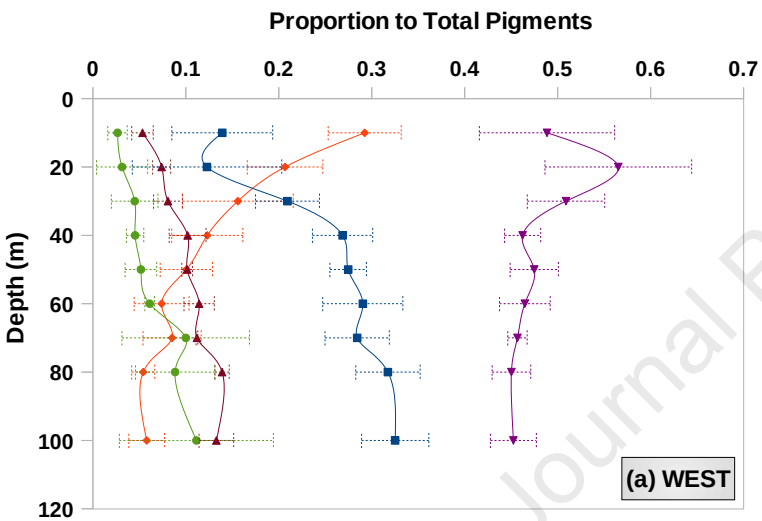

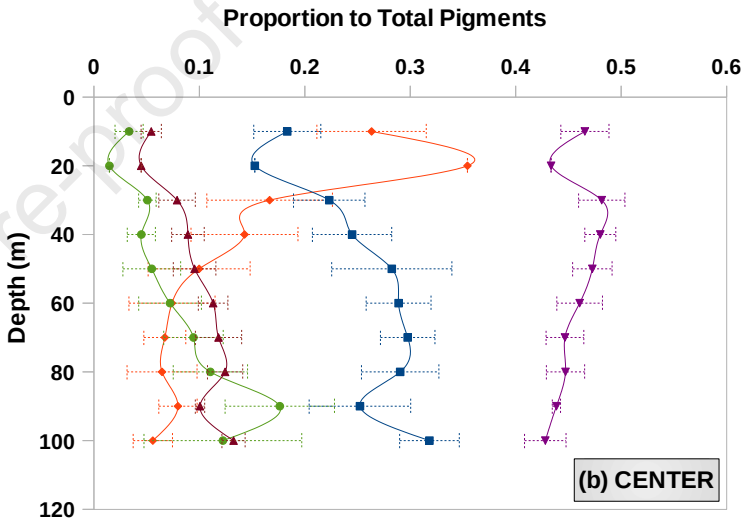

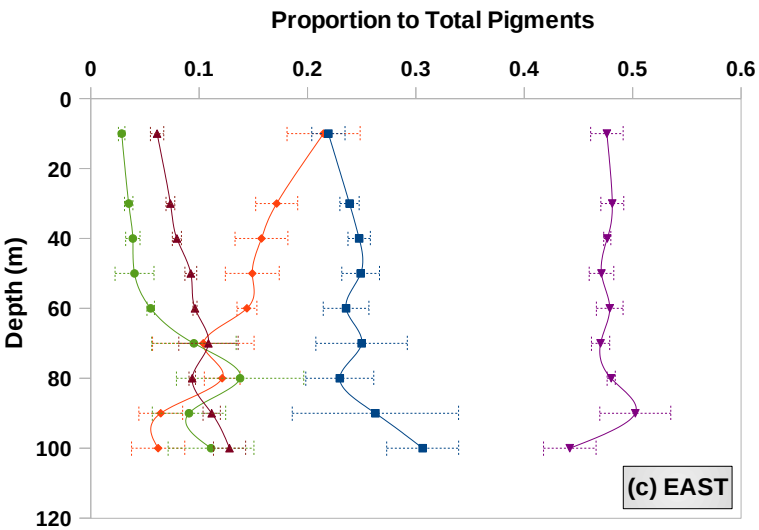

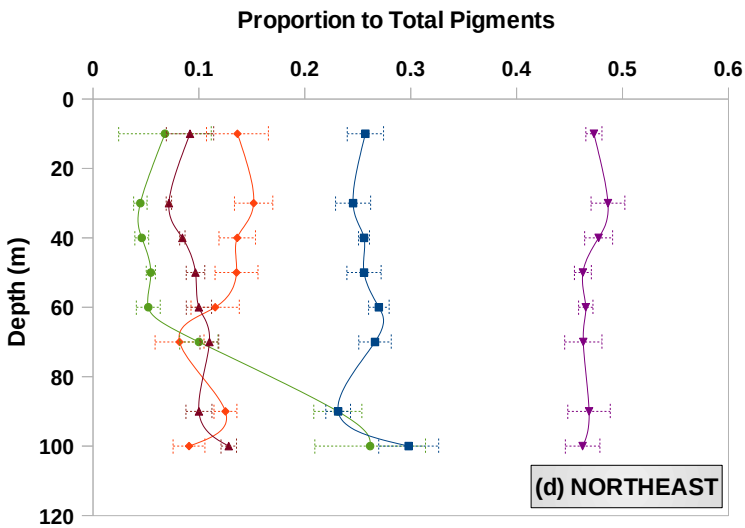

PSC/Tpig TChlc/Tpig TChlb/Tpig TChla/Tpig PPC/Tpig

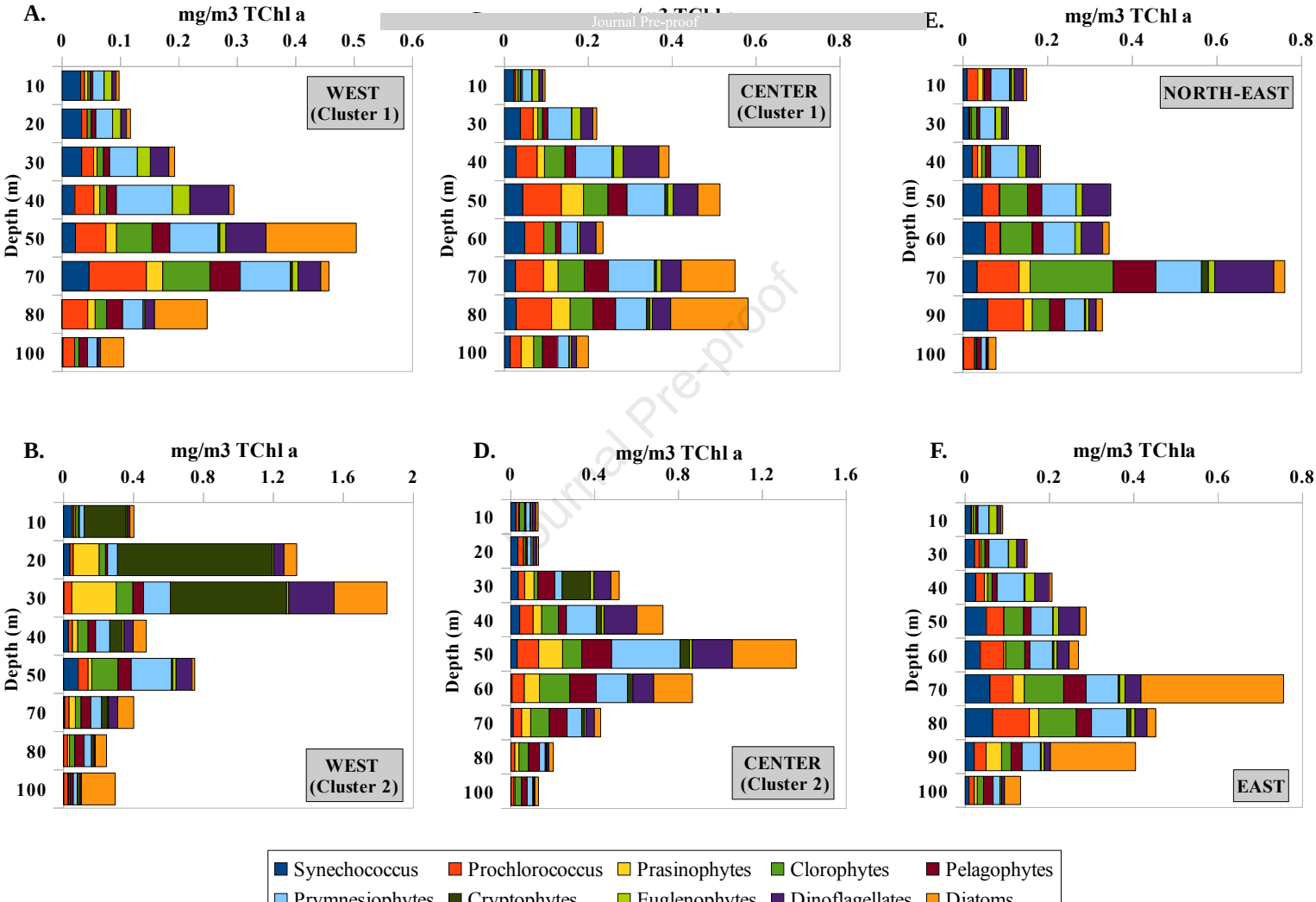

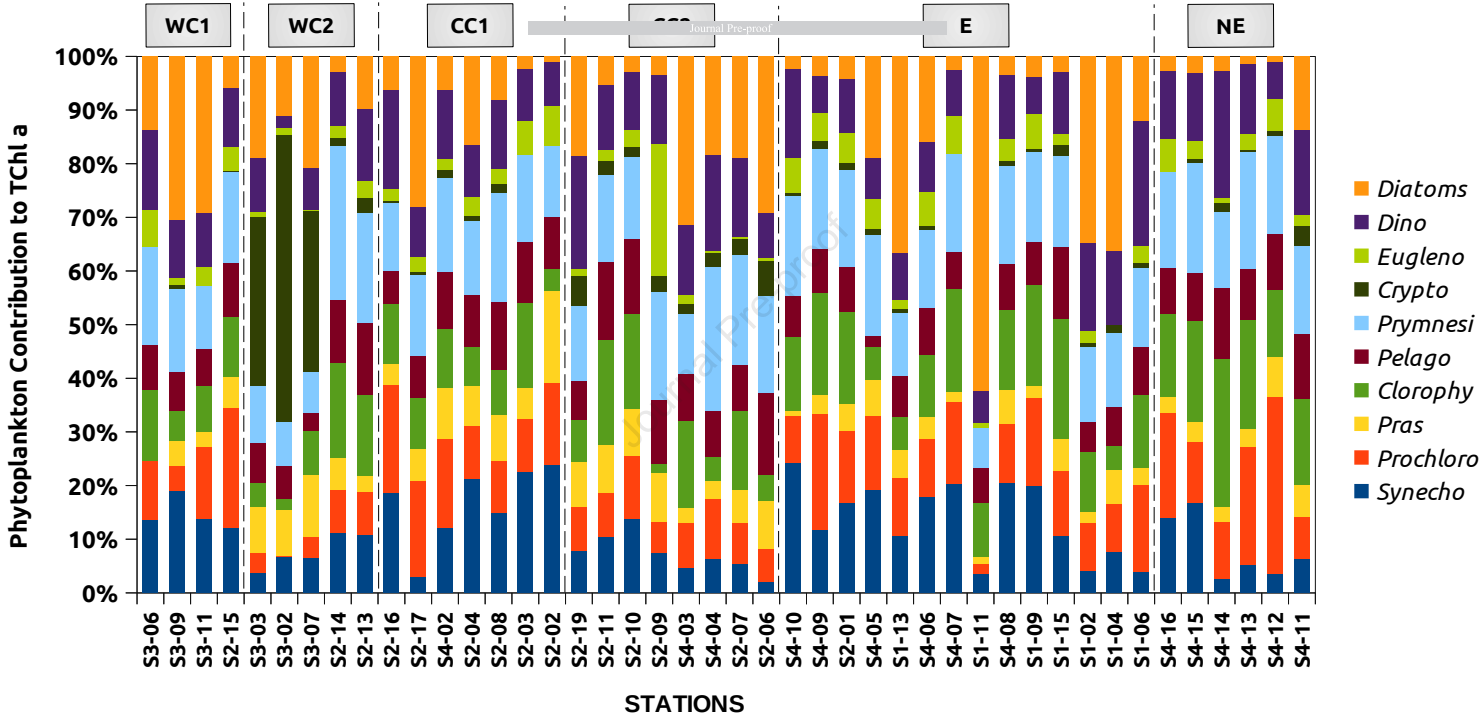
WC1
WC2
CC1
E
NE
Phytoplankton Contribution to TChl a
100%
90%
80%
70%
60%
50%
40%
30%
20%
10%
0%
S3-06
S3-09
S3-11
S2-15
S3-03
S3-02
S3-07
S2-14
S2-13
S2-16
S2-17
S4-02
S2-04
S2-08
S2-03
S2-02
S2-19
S2-11
S2-10
S2-09
S4-03
S4-04
S2-07
S2-06
S4-10
S4-09
S2-01
S4-05
S1-13
S4-06
S4-07
S1-11
S4-08
S1-09
S1-15
S1-02
S1-04
S1-06
S4-16
S4-15
S4-14
S4-13
S4-12
S4-11
STATIONS
Diatoms
Dino
Eugleno
Crypto
Prymnesi
Pelago
Clorophy
Pras
Prochloro
Synecho

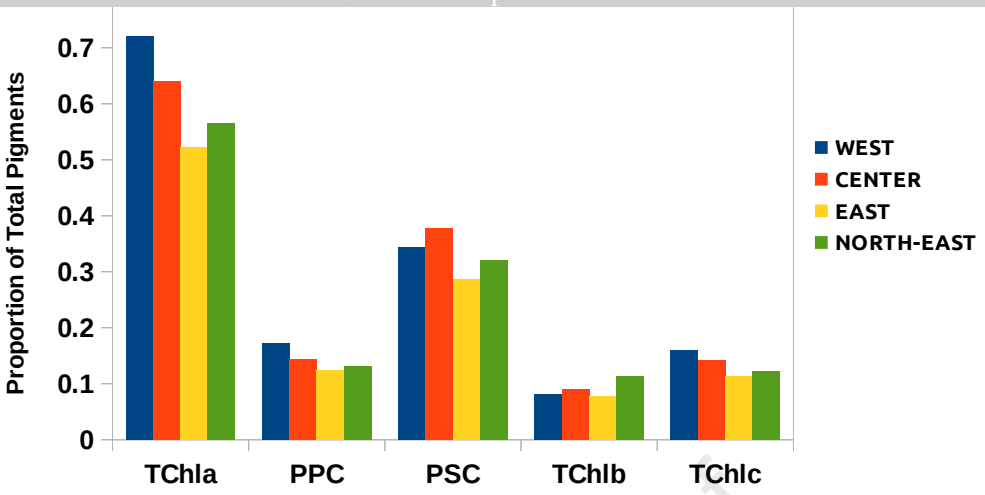

B.

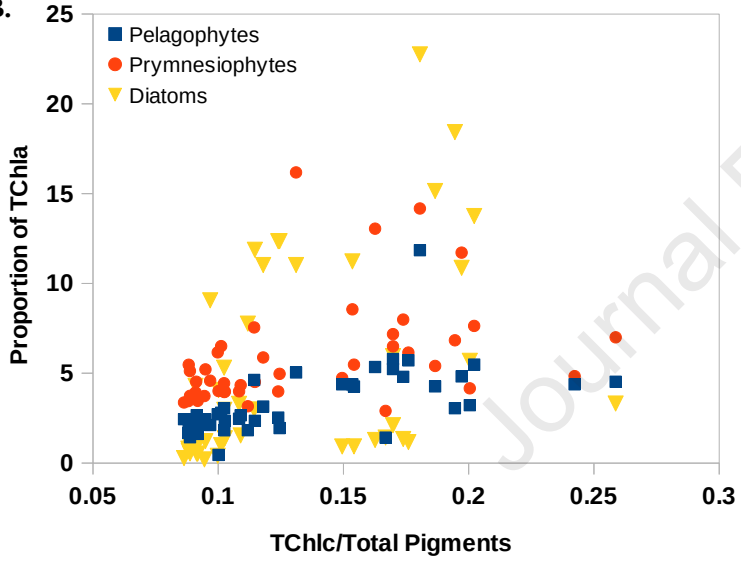

C.

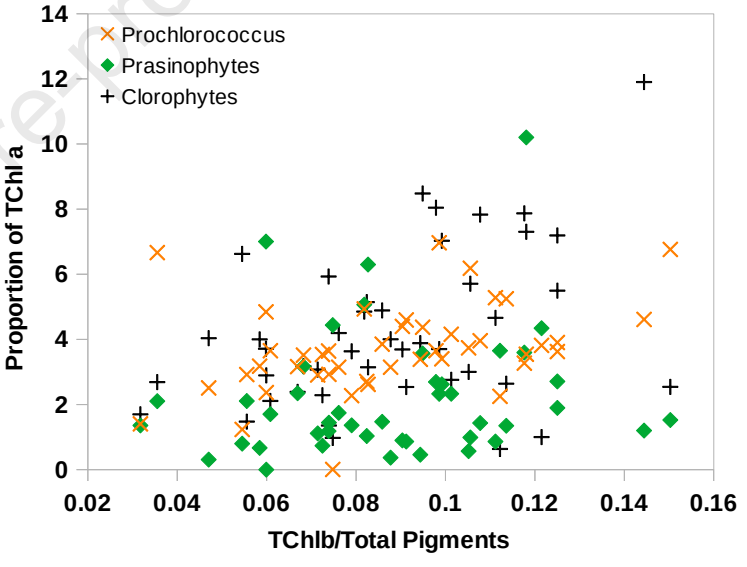

D.

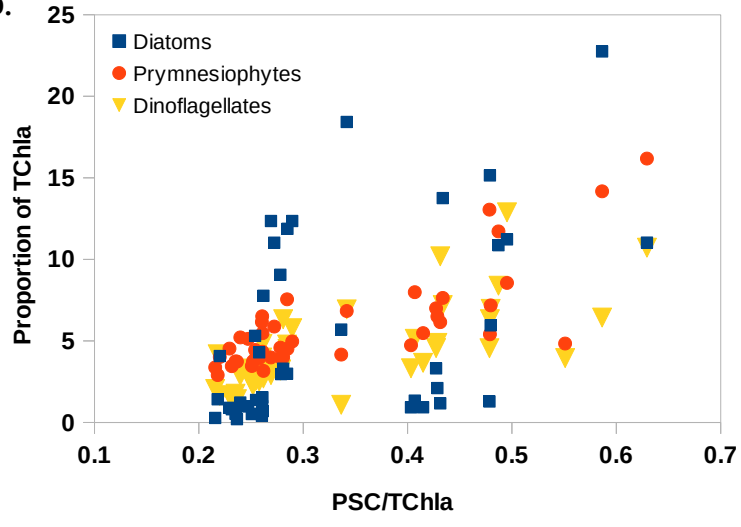

E.

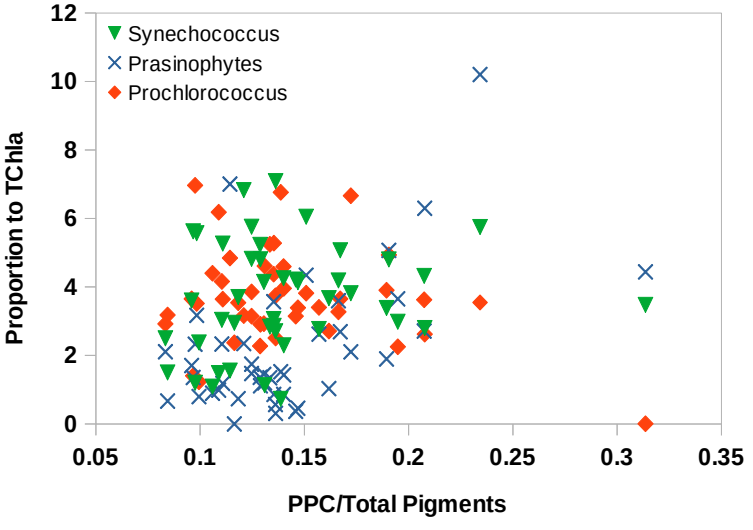

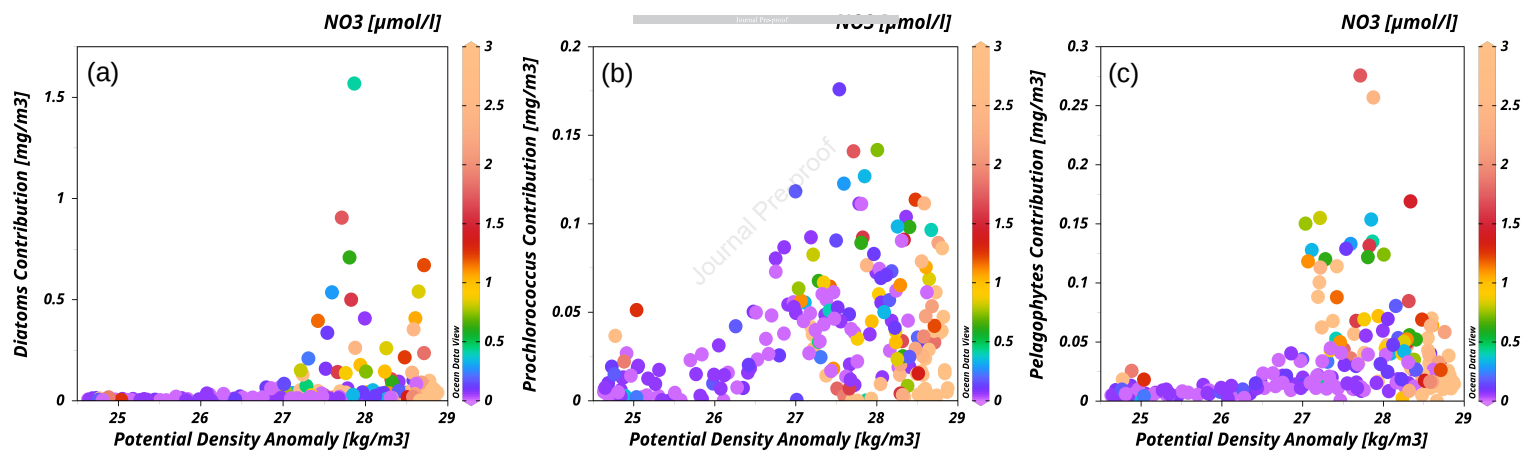
NO3 [µmol/l]
(a)
Diatoms Contribution [mg/m3]
Potential Density Anomaly [kg/m3]
(b)
Prochlorococcus Contribution [mg/m3]
Potential Density Anomaly [kg/m3]
(c)
Pelagophytes Contribution [mg/m3]
Potential Density Anomaly [kg/m3]
Ocean Data View
Journal Preproof

Highlights

- Phytoplankton communities in the Algerian basin are characterized by the CHEMTAX approach.
- Nano- and micro-phytoplankton prevail in the Algerian basin.
- Diatoms, prymnesiophytes, and *Prochlorococcus* are the major phytoplankton groups in the Algerian basin.
- Phytoplankton communities are more abundant and diverse in the western part of the Algerian basin compared to the eastern part.
- The composition of phytoplankton communities is linked to the physical-chemical dynamics of the Algerian basin.

Declaration of interests

☒ The authors declare that they have no known competing financial interests or personal relationships that could have appeared to influence the work reported in this paper.

☐ The authors declare the following financial interests/personal relationships which may be considered as potential competing interests: